

# Full optimization of quasiharmonic free energy with an anharmonic lattice model: Application to thermal expansion and pyroelectricity of wurtzite GaN and ZnO

Ryota Masuki<sup>1,\*</sup>, Takuya Nomoto<sup>2,†</sup>, Ryotaro Arita<sup>2,3,‡</sup> and Terumasa Tadano<sup>4,§</sup>

<sup>1</sup>*Department of Applied Physics, The University of Tokyo, 7-3-1 Hongo, Bunkyo-ku, Tokyo 113-8656, Japan*

<sup>2</sup>*Research Center for Advanced Science and Technology, The University of Tokyo, 4-6-1 Komaba Meguro-ku, Tokyo 153-8904, Japan*

<sup>3</sup>*RIKEN Center for Emergent Matter Science, 2-1 Hirosawa, Wako, Saitama 351-0198, Japan*

<sup>4</sup>*CMSM, National Institute for Materials Science, 1-2-1 Sengen, Tsukuba, Ibaraki 305-0047, Japan*



(Received 12 February 2023; accepted 6 April 2023; published 26 April 2023)

We present a theory and a calculation scheme of structural optimization at finite temperatures within the quasiharmonic approximation (QHA). The theory is based on an efficient scheme of updating the interatomic force constants (IFCs) with the change of crystal structures, which we call the IFC renormalization. The cell shape and the atomic coordinates are treated equally and simultaneously optimized. We apply the theory to the thermal expansion and the pyroelectricity of wurtzite GaN and ZnO, which accurately reproduces the experimentally observed behaviors. Furthermore, we point out a general scheme to obtain correct  $T$  dependence at the lowest order in constrained optimizations that reduce the number of effective degrees of freedom, which is helpful to perform efficient QHA calculations with little sacrificing of accuracy. We show that the scheme works properly for GaN and ZnO by comparing with the optimization of all the degrees of freedom.

DOI: [10.1103/PhysRevB.107.134119](https://doi.org/10.1103/PhysRevB.107.134119)

## I. INTRODUCTION

The thermophysical properties are among the most basic properties of solids, which play an important role in both fundamental science and various applications [1–6]. For its significant consequences, such as the thermal expansion and the pyroelectricity, it is essential to develop quantitative first-principles methods to understand and predict materials with desired properties.

The quasiharmonic approximation (QHA) is a widely used method [7–11] that accurately computes the  $T$ -dependent crystal structure of weakly anharmonic solids [12–14]. In QHA, we neglect the anharmonic effect except for the crystal-structure dependence of the phonon frequencies  $\{\hbar\omega_{k\lambda}\}$  and approximate the free energy by the harmonic one [15–17]. The temperature-dependent crystal structure is obtained by minimizing the free energy with respect to the relevant structural degrees of freedom. In the simple implementation, the phonon frequencies are calculated on a grid in the parameter space, and the free energy is fitted to calculate the temperature-dependent optimal parameters [9,17–19]. This method works efficiently in optimizing a single degree of freedom, such as the lattice constant of a cubic material [17,20,21]. However, the computational cost exponentially increases with the number of degrees of freedom  $N_{\text{param}}$  because the phonon calculations must be performed on a multidimensional grid.

Several constrained optimization schemes have been proposed that reduce the number of effective degrees of freedom to perform calculations efficiently. Using strain-dependent internal coordinates, which are determined to minimize the static potential energy, is the zero static internal stress approximation (ZSISA) [22–24]. ZSISA is correct for the  $T$ -dependent strain at the lowest order [22]. ZSISA combined with finite-temperature corrections of atomic shifts is used for calculating the pyroelectricity [23], which is actively studied recently [25–27]. In further approximation, the free energy is optimized with respect to the volume, while the other degrees of freedom are determined to minimize the static energy at fixed volumes [11,28–31]. Based on these constrained optimizations, computational methods have also been devised to decrease computational costs further. The methods that use the Taylor expansion of the QHA free energy [32,33] or the phonon frequencies [30] and those focused on the irreducible representations of the symmetry groups are proposed [34]. However, the internal coordinates are not optimized independently from the strain in these methods.

In this paper, we develop a theory and a calculation scheme to optimize all the external and internal degrees of freedom within the quasiharmonic approximation. Our method is based on the interatomic force constant (IFC) renormalization, which efficiently updates the IFCs using the anharmonic force constants [35,36]. Due to the compressive sensing method, which enables efficient extraction of the higher-order IFCs from a small number of displacement-force data [37–39], the computational cost does not drastically increase for materials with many internal degrees of freedom. We apply the method to predict the thermal expansion and the pyroelectricity of wurtzite GaN and ZnO, for which we obtain reasonable agreements with the experimental results. The wurtzite materials

\*masuki-ryota774@g.ecc.u-tokyo.ac.jp

†nomoto@ap.t.u-tokyo.ac.jp

‡arita@riken.jp

§tadano.terumasa@nims.go.jp

have two independent lattice constants and an internal degree of freedom which is coupled to the electric polarization. The magnitude of anharmonicity is moderate in these materials, thus the  $T$ -dependent crystal structures are correctly described by QHA [40].

Furthermore, we prove a general theorem that provides an important guideline to efficiently get reliable results in constrained QHA optimizations. The theorem is mathematically a straightforward generalization of a previous result on ZSISA [22], but it is helpful in designing constrained optimization schemes and clarifying their range of applicability. Using the theorem, it is possible to get reasonable finite-temperature structures with  $N_{\text{param}}$  separate one-dimensional optimizations instead of the grid search on  $N_{\text{param}}$ -dimensional parameter space, which decreases the computational cost from  $O(N_s^{N_{\text{param}}})$  to  $O(N_s N_{\text{param}})$ , where  $N_s$  is the number of sampling points of each parameter. We implement ZSISA and several other constrained optimizations, whose results support the general statement. Note that the pyroelectricity is suitable to demonstrate the theory because the  $T$  dependence of atomic positions needs to be investigated.

## II. THEORY

### A. QHA

The anharmonic effect at each structure is neglected in the QHA. Thus, the QHA free energy of a crystal structure given by  $X$  can be written as

$$F_{\text{QHA}}(X, T) = U_0(X) + \sum_{k\lambda} \left[ \frac{1}{2} \hbar \omega_{k\lambda}(X) + k_B T \log(1 - e^{-\beta \hbar \omega_{k\lambda}(X)}) \right], \quad (1)$$

where  $U_0(X)$  is the electronic ground state energy and  $\omega_{k\lambda}(X)$  is the  $X$ -dependent harmonic phonon frequency.  $X$  consists of the external strain and the internal atomic positions. The crystal structure at finite temperature  $T$  can be obtained by minimizing the QHA free energy as

$$X(T) = \underset{X}{\operatorname{argmin}} F_{\text{QHA}}(X, T). \quad (2)$$

When combined with first-principles calculations, the most time-consuming part is the calculation of the structure dependence of the harmonic phonon frequencies  $\omega_{k\lambda}(X)$ .

### B. IFC renormalization

We start from the Taylor expansion of the potential energy surface, which is introduced in Sec. I in the Supplemental Material [41]. The IFC renormalization is a calculation method to update the set of IFCs when the crystal structure is changed [35,36]. Since the new set of IFCs is calculated from the IFCs in the reference structure, there is no need to run additional electronic structure calculations at every step of the structure update, which makes the calculation significantly efficient.

The change of crystal structures can be described by the combination of the strain and the atomic displacements. We write the static atomic displacement in normal coordinate representation as

$$q_\lambda^{(0)} = \sum_{\alpha\mu} \epsilon_{0\lambda,\alpha\mu} \sqrt{M_\alpha} u_{\alpha\mu}^{(0)}, \quad (3)$$

where  $u_{\alpha\mu}^{(0)}$  is the  $\mu (= x, y, z)$  component of the static displacement of atom  $\alpha$ .  $M_\alpha$  is the mass of atom  $\alpha$  and  $\epsilon_{0\lambda,\alpha\mu}$  is the polarization vector of the mode  $\lambda$  at the  $\Gamma$  point.  $u_{\alpha\mu}^{(0)}$  is independent of the primitive cell  $\mathbf{R}$  because we assume that the temperature-induced structural change is commensurate to the  $\Gamma$  point in the Brillouin zone.

As for the strain, we use the displacement gradient tensor  $u_{\mu\nu}$  as the basic variable, which is defined as

$$u_{\mu\nu} = \frac{\partial \tilde{x}_\mu}{\partial x_\nu} - \delta_{\mu\nu} \quad (4)$$

if the atom at  $\mathbf{x}$  is moved to  $\tilde{\mathbf{x}}$  by the strain. We restrict  $u_{\mu\nu}$  to be symmetric to fix the rotational degrees of freedom.

The structural change described by the atomic displacements  $q_\lambda^{(0)}$  corresponds to changing the center in the Taylor expansion of Eqs. (S1) and (S2) in the Supplemental Material [41]. As we have the polynomial form of the potential energy surface, which is determined by the IFCs at the reference structure, it is possible to Taylor expand again around the new structure. The expansion coefficient at the updated structure given by  $q^{(0)}$  is written as

$$\begin{aligned} \tilde{\Phi}^{(q^{(0)})}(\mathbf{k}_1\lambda_1, \dots, \mathbf{k}_n\lambda_n) &= \sum_{m=0}^{\infty} \frac{1}{m!} \sum_{\{\rho\}} \tilde{\Phi}^{(q^{(0)}=0)}(\mathbf{k}_1\lambda_1, \dots, \mathbf{k}_n\lambda_n, \mathbf{0}\rho_1, \dots, \mathbf{0}\rho_m) \\ &\quad \times q_{\rho_1}^{(0)} \dots q_{\rho_m}^{(0)}. \end{aligned} \quad (5)$$

The derivation of the corresponding formula for the strain is more complicated. Although the strain is not included in the Taylor expansion of the potential energy surface [Eqs. (S1) and (S2) in the Supplemental Material [41]], it is possible to recapture the strain as a set of static atomic displacements:

$$u_{\mathbf{R}\alpha\mu}^{(0)} = \sum_{\nu} u_{\mu\nu} (R_\nu + d_{\alpha\nu}) = \sum_{\nu} u_{\mu\nu} R_{\alpha\nu}, \quad (6)$$

where  $\mathbf{d}_\alpha$  is the position of the atom  $\alpha$  in the primitive cell. We define  $\mathbf{R}_\alpha = \mathbf{R} + \mathbf{d}_\alpha$  for notational simplicity. Thus, we can derive the IFC renormalization in terms of strain as

$$\begin{aligned} \Phi_{\mu_1 \dots \mu_n}^{(u_{\mu\nu})}(\mathbf{R}_1\alpha_1, \dots, \mathbf{R}_n\alpha_n) &= \sum_{m=0}^{\infty} \frac{1}{m!} \sum_{\{\mathbf{R}'\alpha'\mu'\nu'\}} \Phi_{\mu_1 \dots \mu_n \mu'_1 \dots \mu'_m}^{(u_{\mu\nu}=0)}(\mathbf{R}_1\alpha_1, \dots, \mathbf{R}_n\alpha_n, \mathbf{R}'_1\alpha'_1, \dots, \mathbf{R}'_m\alpha'_m) \\ &\quad \times u_{\mu'_1\nu'_1} R'_{1\alpha'_1\nu'_1} \dots u_{\mu'_m\nu'_m} R'_{m\alpha'_m\nu'_m}. \end{aligned} \quad (7)$$

See Ref. [35] for more detailed explanations. Using Eqs. (5) and (7), we can get the updated IFCs for arbitrary strain

and atomic displacements as long as the expansion from the reference structure is valid. Hereafter,  $\Phi$  and  $\tilde{\Phi}$  without notes in superscripts denote the renormalized IFCs  $\Phi^{(q^{(0)}, u_{\mu\nu})}$  and  $\tilde{\Phi}^{(q^{(0)}, u_{\mu\nu})}$ , respectively, unless otherwise stated.

In the calculation, we truncate the Taylor expansion at the fourth order. As the IFC renormalization by strain [Eq. (7)] is written down in the real space, we first calculate them and Fourier transform to the reciprocal space. The IFC renormalization is performed in the order of  $\tilde{\Phi}^{(q^{(0)}=0, u_{\mu\nu}=0)} \rightarrow \tilde{\Phi}^{(q^{(0)}=0, u_{\mu\nu})} \rightarrow \tilde{\Phi}^{(q^{(0)}, u_{\mu\nu})}$ . The details of the procedure are explained in Ref. [35]

Here, it should be noted that Eq. (7) is not directly applicable to the case  $n = 0$  because of the surface effect of the Born–von Kármán supercell [36], which we explain with an example in Sec. II in the Supplemental Material [41]. As the solution for this problem is highly complicated, we expand the strain dependence of the potential energy surface as

$$\begin{aligned} \frac{1}{N} U_0^{(q^{(0)}=0, u_{\mu\nu})} &= \frac{1}{2} \sum_{\mu_1 \nu_1, \mu_2 \nu_2} C_{\mu_1 \nu_1, \mu_2 \nu_2} \eta_{\mu_1 \nu_1} \eta_{\mu_2 \nu_2} \\ &+ \frac{1}{6} \sum_{\mu_1 \nu_1, \mu_2 \nu_2, \mu_3 \nu_3} C_{\mu_1 \nu_1, \mu_2 \nu_2, \mu_3 \nu_3} \eta_{\mu_1 \nu_1} \eta_{\mu_2 \nu_2} \eta_{\mu_3 \nu_3} \\ &+ \dots, \end{aligned} \quad (8)$$

where  $N$  is the number of primitive cells in the Born–von Kármán supercell and

$$C_{\mu_1 \nu_1, \mu_2 \nu_2} = \frac{1}{N} \frac{\partial^2 U_0}{\partial \eta_{\mu_1 \nu_1} \partial \eta_{\mu_2 \nu_2}}, \quad (9)$$

$$C_{\mu_1 \nu_1, \mu_2 \nu_2, \mu_3 \nu_3} = \frac{1}{N} \frac{\partial^2 U_0}{\partial \eta_{\mu_1 \nu_1} \partial \eta_{\mu_2 \nu_2} \partial \eta_{\mu_3 \nu_3}} \quad (10)$$

are the second- and third-order elastic constants, which we define as the quantity per unit cell, and

$$\eta_{\mu\nu} = \frac{1}{2} \left[ \sum_{\mu'} (\delta_{\mu\mu'} + u_{\mu\mu'}) (\delta_{\nu\nu'} + u_{\nu\nu'}) - \delta_{\mu\nu} \right] \quad (11)$$

$$= \frac{1}{2} \left( u_{\mu\nu} + u_{\nu\mu} + \sum_{\mu'} u_{\mu\mu'} u_{\nu\nu'} \right) \quad (12)$$

is the strain tensor. The elastic constants are truncated at the third order in our calculation.

The IFC renormalization in terms of atomic displacements [Eq. (5)] does not affect the fitting accuracy of the potential energy surface because it does not alter the potential landscape. However, the IFC renormalization by strain [Eq. (7)] is not necessarily precise because the information in a deformed cell is not provided in calculating the IFCs in the reference structure. Thus, we estimate the coupling between the strain and the harmonic IFCs

$$\frac{\partial \Phi_{\mu_1 \mu_2}(\mathbf{R}_1 \alpha_1, \mathbf{R}_2 \alpha_2)}{\partial u_{\mu\nu}}, \quad (13)$$

using the finite displacement method with respect to the strain [35] to improve the accuracy of the method.

Additionally, the coupling between the first-order IFCs and the strain,

$$\frac{\partial \Phi(\mathbf{0}\lambda)}{\partial u_{\mu\nu}}, \quad (14)$$

is also estimated using the finite displacement method of strain. This is because the acoustic sum rule of the first-order IFCs is broken if the rotational invariance is not imposed on the harmonic IFCs, which we explain in Appendix A. Since the rotational invariance imposes restrictions on IFCs that the atomic forces calculated in the density functional theory (DFT) supercell do not satisfy, it causes unreasonable shifts of the phonon frequencies. The frequency shifts depend on crystal symmetries, which makes the finite displacement estimation of  $\frac{\partial \Phi_{\mu_1 \mu_2}(\mathbf{R}_1 \alpha_1, \mathbf{R}_2 \alpha_2)}{\partial u_{\mu\nu}}$  difficult. Thus, we do not impose the rotational invariance on the harmonic IFCs and calculate  $\frac{\partial \Phi(\mathbf{0}\lambda)}{\partial u_{\mu\nu}}$  using the finite displacement method instead.

The higher-order derivatives  $\frac{\partial^2 \Phi(\mathbf{0}\lambda)}{\partial u_{\mu\nu} \partial u_{\mu'\nu'}}$  and  $\frac{\partial^3 \Phi(\mathbf{0}\lambda)}{\partial u_{\mu_1 \nu_1} \partial u_{\mu_2 \nu_2} \partial u_{\mu_3 \nu_3}}$  are set to zero because the rotational invariance of the higher-order IFCs is required for them to satisfy the acoustic sum rule, which we also discuss in Appendix A.

### C. Structural optimization within QHA

Using the IFC renormalization, the harmonic phonon dispersion and their derivatives can be calculated for updated crystal structures, which enables efficient minimization of the QHA free energy. We begin with introducing a notation for the mode transformation. From here on, we distinguish the phonon modes in the reference structure and those in the updated structure. The former, which we write with greek letters without a bar (such as  $\lambda$ ), is obtained by diagonalizing the dynamical matrix in the reference structure:

$$\begin{aligned} \sum_{\beta\nu} \left[ \frac{1}{\sqrt{M_\alpha M_\beta}} \sum_{\mathbf{R}} \Phi_{\mu\nu}^{(q^{(0)}=0, u_{\mu\nu}=0)}(\mathbf{0}\alpha, \mathbf{R}\beta) e^{i\mathbf{k}\cdot\mathbf{R}} \right] \epsilon_{\mathbf{k}\lambda, \beta\nu} \\ = \omega_{\mathbf{k}\lambda}^2 \epsilon_{\mathbf{k}\lambda, \alpha\mu}. \end{aligned} \quad (15)$$

These modes are fixed throughout the calculation, which serves as a reference frame. The phonon modes in an updated structure, which we denote with a bar like  $\bar{\lambda}$ , diagonalize the dynamical matrix in the updated structure. We define the mode transformation matrix

$$C_{\mathbf{k}\lambda\bar{\lambda}} = \sum_{\alpha\mu} \epsilon_{\mathbf{k}\lambda, \alpha\mu}^* \epsilon_{\mathbf{k}\bar{\lambda}, \alpha\mu}. \quad (16)$$

Let us calculate the derivatives of the QHA free energy using the mode transformation. Considering that the dynamical matrix is dependent on a parameter  $s$ , we can derive the formula

$$\frac{\partial(\omega_{\mathbf{k}\bar{\lambda}}^2)}{\partial s} = \sum_{\lambda_1 \lambda_2} C_{\mathbf{k}\lambda_1 \bar{\lambda}}^* \frac{\partial \tilde{\Phi}(-\mathbf{k}\lambda_1, \mathbf{k}\lambda_2)}{\partial s} C_{\mathbf{k}\lambda_2 \bar{\lambda}}. \quad (17)$$

Substituting  $s = \tilde{\Phi}(-\mathbf{k}\lambda_1, \mathbf{k}\lambda_2)$ , we get

$$\frac{\partial(\omega_{\mathbf{k}\bar{\lambda}})}{\partial\tilde{\Phi}(-\mathbf{k}\lambda_1, \mathbf{k}\lambda_2)} = \frac{C_{\mathbf{k}\lambda_1\bar{\lambda}}^* C_{\mathbf{k}\lambda_2\bar{\lambda}}}{2\omega_{\mathbf{k}\bar{\lambda}}}. \quad (18)$$

Therefore, for a general structural degree of freedom  $X_i$  that describes the atomic displacement  $q_\lambda^{(0)}$  or the strain  $u_{\mu\nu}$ , the derivative of the QHA free energy can be calculated as

$$\begin{aligned} \frac{\partial F_{\text{QHA}}(X, T)}{\partial X_i} &= \frac{\partial U_0}{\partial X_i} \\ &+ \sum_{\mathbf{k}\bar{\lambda}\lambda_1\lambda_2} \frac{\hbar n_B(\hbar\omega_{\mathbf{k}\bar{\lambda}}) + 1/2}{\omega_{\mathbf{k}\bar{\lambda}}} C_{\mathbf{k}\lambda_1\bar{\lambda}}^* \\ &\times C_{\mathbf{k}\lambda_2\bar{\lambda}} \frac{\partial\tilde{\Phi}(-\mathbf{k}\lambda_1, \mathbf{k}\lambda_2)}{\partial X_i}. \end{aligned} \quad (19)$$

The derivatives  $\frac{\partial U_0}{\partial X_i}$  and  $\frac{\partial\tilde{\Phi}(-\mathbf{k}\lambda_1, \mathbf{k}\lambda_2)}{\partial X_i}$  can be obtained by differentiating Eqs. (5), (7), and (8).

In our calculation, where the IFCs are truncated at the fourth order and the elastic constants at the third order, the corresponding formulas are written as

$$\frac{1}{N} \frac{\partial U_0^{(q^{(0)}, u_{\mu\nu})}}{\partial q_\lambda^{(0)}} = \tilde{\Phi}^{(q^{(0)}, u_{\mu\nu})}(\mathbf{0}\lambda), \quad (20)$$

$$\frac{\partial\tilde{\Phi}^{(q^{(0)}, u_{\mu\nu})}(\mathbf{k}_1\lambda_1, -\mathbf{k}_1\lambda_2)}{\partial q_\lambda^{(0)}} = \tilde{\Phi}^{(q^{(0)}, u_{\mu\nu})}(\mathbf{k}_1\lambda_1, -\mathbf{k}_1\lambda_2, \mathbf{0}\lambda), \quad (21)$$

$$\begin{aligned} \frac{1}{N} \frac{\partial U_0^{(q^{(0)}, u_{\mu\nu})}}{\partial u_{\mu\nu}} &= \sum_{\mu'v'} \frac{\partial\eta_{\mu'v'}}{\partial u_{\mu\nu}} \left( \sum_{\mu_1v_1} C_{\mu_1v_1, \mu'v'} \eta_{\mu_1v_1} \right. \\ &+ \frac{1}{2} \sum_{\mu_1v_1, \mu_2v_2} C_{\mu_1v_1, \mu_2v_2, \mu'v'} \eta_{\mu_1v_1} \eta_{\mu_2v_2} \left. \right) \\ &+ \sum_{m=1}^3 \frac{1}{m!} \sum_{\{\lambda\}} \frac{\partial\tilde{\Phi}^{(q^{(0)}=0, u_{\mu\nu})}(\mathbf{0}\lambda_1, \dots, \mathbf{0}\lambda_m)}{\partial u_{\mu\nu}} \\ &\times q_{\lambda_1}^{(0)} \cdots q_{\lambda_m}^{(0)}, \end{aligned} \quad (22)$$

$$\begin{aligned} \frac{\partial\tilde{\Phi}^{(q^{(0)}, u_{\mu\nu})}(\mathbf{k}_1\lambda_1, -\mathbf{k}_1\lambda_2)}{\partial u_{\mu\nu}} &= \frac{\partial\tilde{\Phi}(\mathbf{k}_1\lambda_1, -\mathbf{k}_1\lambda_2)}{\partial u_{\mu\nu}} \\ &+ \sum_{\mu'v'} \frac{\partial^2\tilde{\Phi}(\mathbf{k}_1\lambda_1, -\mathbf{k}_1\lambda_2)}{\partial u_{\mu\nu} \partial u_{\mu'v'}} u_{\mu'v'} \\ &+ \sum_{\rho_1} \frac{\partial\tilde{\Phi}(\mathbf{k}_1\lambda_1, -\mathbf{k}_1\lambda_2, \mathbf{0}\rho_1)}{\partial u_{\mu\nu}} q_{\rho_1}^{(0)}, \end{aligned} \quad (23)$$

for the internal coordinates and the strain, respectively. The derivatives of the IFCs in the right-hand side of Eq. (23) are estimated at the reference structure ( $q_\lambda^{(0)} = 0, u_{\mu\nu} = 0$ ).

Using the gradients of the free energy, we can simultaneously optimize all the internal and external degrees of freedom to minimize the QHA free energy. We denote the difference of the crystal structure from the optimum structure by  $\delta q_\lambda^{(0)}$  and

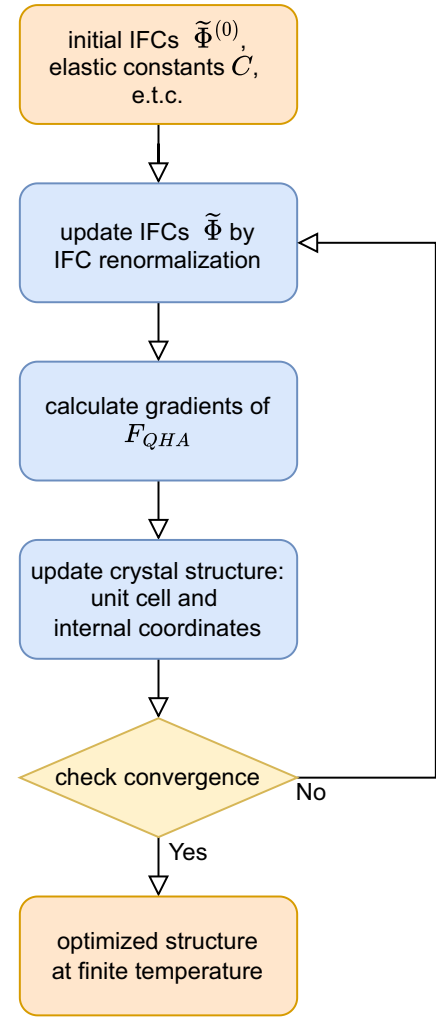


FIG. 1. The calculation flow of the finite-temperature structural optimization within the quasiharmonic approximation combined with the IFC renormalization.

$\delta u_{\mu\nu}$ . These quantities can be estimated by solving the linear equations

$$\frac{1}{N} \frac{\partial F_{\text{QHA}}}{\partial q_\lambda^{(0)}} = \sum_{\lambda_1} \tilde{\Phi}(\mathbf{0}\lambda, \mathbf{0}\lambda_1) \delta q_{\lambda_1}^{(0)}, \quad (24)$$

$$\frac{1}{N} \frac{\partial F_{\text{QHA}}}{\partial u_{\mu\nu}} = \sum_{\mu_1v_1} C_{\mu\nu, \mu_1v_1} \delta u_{\mu_1v_1}, \quad (25)$$

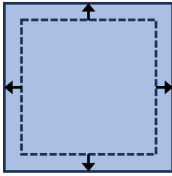
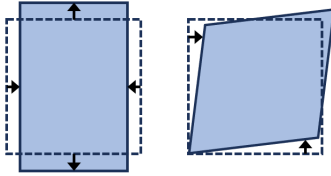
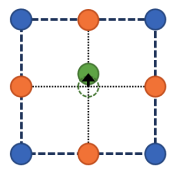
where we approximate the Hessian of the QHA free energy by  $\tilde{\Phi}(\mathbf{0}\lambda, \mathbf{0}\lambda_1)$  and  $C_{\mu\nu, \mu_1v_1}$ . We assume that  $u_{\mu\nu}$  is symmetric to fix the rotational degrees of freedom, which is necessary to get a unique solution of Eq. (25). The crystal structures are updated by

$$q_\lambda^{(0)} \leftarrow q_\lambda^{(0)} - \beta_{\text{mix,ion}} \delta q_\lambda^{(0)}, \quad (26)$$

$$u_{\mu\nu} \leftarrow u_{\mu\nu} - \beta_{\text{mix,cell}} \delta u_{\mu\nu}. \quad (27)$$

The coefficients  $\beta_{\text{mix,ion}}$  and  $\beta_{\text{mix,cell}}$  are introduced for robust convergence of the calculation. As for the constrained optimization methods such as ZSISA, we formulate different

TABLE I. The schematic explanation of some different optimization schemes of QHA. Full optimization is the simultaneous optimization of all the degrees of freedom. In the table, QHA means that the degree of freedom is optimized at finite temperatures to minimize the QHA free energy, whereas static means that the degree of freedom is optimized in the static potential energy surface, which does not include the contribution of the lattice vibrations.

	cell volume	deviatoric strain	atomic positions
			
full optimization	QHA	QHA	QHA
ZSISA	QHA	QHA	static
v-ZSISA	QHA	static	static

schemes of updating the crystal structure, which are described in detail in Appendix B.

From the above discussions, the calculation flow of the structural optimization based on IFC renormalization and QHA is as follows, which we illustrate in Fig. 1.

- (1) Input IFCs, elastic constants, etc., at the reference structure. Define the initial structure.
- (2) Calculate the IFCs in the current structure by IFC renormalization.
- (3) Calculate gradients of the QHA free energy [Eqs. (19)–(23)].
- (4) Update the crystal structure [Eqs. (24)–(27)].
- (5) Check convergence. If the convergence has yet to be achieved, go to (2).

We implement the theory to the ALAMODE package [37,42,43], which is an open-source software for anharmonic phonon calculation. The developed feature will be made public in its future release.

#### D. General scheme of constrained optimizations correct at the lowest order

Due to the high computational cost of optimizing all the degrees of freedom, numerous constrained optimization schemes have been proposed to decrease the number of effective degrees of freedom. ZSISA, which uses strain-dependent static internal coordinates [22], is a representative example. In further approximation, the internal and deviatoric degrees of freedom are determined by minimizing the static energy [11,28–31], which we call volumetric ZSISA (v-ZSISA). We illustrate ZSISA and v-ZSISA with a schematic in Table I.

Here, we show a general theorem on these constrained optimizations.

*Theorem.* Consider optimizing the QHA free energy with respect to a set of structural degrees of freedom  $\{X_i\}$ . Then, if the other degrees of freedom  $\{\bar{X}_j\}$  are determined to minimize the static energy  $U_0$  for given configurations of  $\{X_i\}$ , the obtained  $T$  dependence of  $\{X_i\}$  agrees at the lowest order with the result of the optimization of all the degrees of freedom (full optimization).

Mathematically, the theorem is just a straightforward corollary of the result in Ref. [22]. However, we discuss it here

because it will be a powerful guiding principle in designing an efficient and accurate constrained scheme of QHA. Before the proof of the theorem, we consider some of its applications, which we summarize in a list below.

(1) In ZSISA,  $\{X_i\}$  represent the strain, and  $\{\bar{X}_j\}$  represent the internal coordinates. The theorem claims that  $T$  dependence of the strain calculated by ZSISA is correct at the lowest order, which has been pointed out in Ref. [22].

(2) In v-ZSISA,  $\{X_i\}$  represent the hydrostatic strain that causes volumetric expansion

$$u_{V,\mu\nu} \simeq \begin{pmatrix} 1 & 0 & 0 \\ 0 & 1 & 0 \\ 0 & 0 & 1 \end{pmatrix}, \quad (28)$$

while  $\{\bar{X}_j\}$  represent the deviatoric strain and the internal coordinates. According to the theorem, the volumetric expansion will be properly reproduced by v-ZSISA.

(3)  $T$  dependence of an arbitrary degree of freedom  $X_i$  can be calculated correctly at the lowest order if we relax all the other degrees of freedom in the static potential. This fact helps reduce the optimization of multiple degrees of freedom to the problem of separate optimization of each degree of freedom. Compared to the  $N_{\text{param}}$ -dimensional grid search of the computational cost of  $O(N_s^{N_{\text{param}}})$ , the computational cost of the separate one-dimensional optimization is decreased to  $O(N_s N_{\text{param}})$ , where  $N_s$  is the number of sampling points of each parameter. For example, consider the calculation of anisotropic expansion determined by two lattice constants,  $a$  and  $c$ . The  $T$  dependence of  $a$  can be calculated by optimizing  $c$  and the internal coordinate in the static potential. The  $T$  dependence of  $c$  can be calculated in a similar one-parameter optimization. The  $T$  dependence of  $c$  in the calculation of  $a$  and that of  $a$  in calculating  $c$  should be disregarded.

It is worth mentioning that these constrained optimizations do not always reproduce the full optimization precisely because the higher-order effects can be non-negligible in actual calculations. Nonetheless, in Secs. IV B and IV C, we discuss that the constrained optimization schemes based on the theorem give qualitatively accurate results more robustly than other schemes, once we determine the degrees of freedom to consider.

We move on to the proof of the theorem. Since we assume that the reference structure is optimized in terms of the static potential  $U_0$ , the Taylor expansion of  $U_0(X, \bar{X})$  is written as

$$\begin{aligned} U_0(X, \bar{X}) &= U_0(X = \bar{X} = 0) + \frac{1}{2} \sum_{i_1 i_2} \frac{\partial^2 U_0}{\partial X_{i_1} \partial X_{i_2}} X_{i_1} X_{i_2} \\ &+ \sum_{ij} \frac{\partial^2 U_0}{\partial X_i \partial \bar{X}_j} X_i \bar{X}_j + \frac{1}{2} \sum_{j_1 j_2} \frac{\partial^2 U_0}{\partial \bar{X}_{j_1} \partial \bar{X}_{j_2}} \bar{X}_{j_1} \bar{X}_{j_2} + \dots \end{aligned} \quad (29)$$

The Taylor expansion of the QHA free energy is

$$\begin{aligned} F_{\text{QHA}}(X, \bar{X}, T) &= F_{\text{QHA}}(X = \bar{X} = 0, T) + \frac{1}{2} \sum_{i_1 i_2} \frac{\partial^2 U_0}{\partial X_{i_1} \partial X_{i_2}} X_{i_1} X_{i_2} \\ &+ \sum_{ij} \frac{\partial^2 U_0}{\partial X_i \partial \bar{X}_j} X_i \bar{X}_j + \frac{1}{2} \sum_{j_1 j_2} \frac{\partial^2 U_0}{\partial \bar{X}_{j_1} \partial \bar{X}_{j_2}} \bar{X}_{j_1} \bar{X}_{j_2} + \dots \\ &+ \sum_i \frac{\partial F_{\text{QHA}}^{\text{vib}}}{\partial X_i} X_i + \sum_j \frac{\partial F_{\text{QHA}}^{\text{vib}}}{\partial \bar{X}_j} \bar{X}_j + \dots \end{aligned} \quad (30)$$

Thus, in the lowest-order approximation, the crystal structure that gives the minimum of the QHA free energy is calculated by solving

$$\begin{pmatrix} \frac{\partial^2 U_0}{\partial X \partial X} & \frac{\partial^2 U_0}{\partial X \partial \bar{X}} \\ \frac{\partial^2 U_0}{\partial \bar{X} \partial X} & \frac{\partial^2 U_0}{\partial \bar{X} \partial \bar{X}} \end{pmatrix} \begin{pmatrix} X \\ \bar{X} \end{pmatrix} = - \begin{pmatrix} \frac{\partial F_{\text{QHA}}^{\text{vib}}}{\partial X} \\ \frac{\partial F_{\text{QHA}}^{\text{vib}}}{\partial \bar{X}} \end{pmatrix}. \quad (31)$$

To eliminate  $\bar{X}$  from the equation, we use

$$\bar{X} = - \left( \frac{\partial^2 U_0}{\partial \bar{X} \partial \bar{X}} \right)^{-1} \left\{ \left( \frac{\partial^2 U_0}{\partial X \partial \bar{X}} \right) X + \left( \frac{\partial F_{\text{QHA}}^{\text{vib}}}{\partial \bar{X}} \right) \right\}, \quad (32)$$

where we abbreviate the subscripts. The derivatives are estimated at  $X = \bar{X} = 0$  in this section, except noted otherwise explicitly. Substituting to Eq. (31), we get

$$\begin{aligned} &\left[ \left( \frac{\partial^2 U_0}{\partial X \partial X} \right) - \left( \frac{\partial^2 U_0}{\partial X \partial \bar{X}} \right) \left( \frac{\partial^2 U_0}{\partial \bar{X} \partial \bar{X}} \right)^{-1} \left( \frac{\partial^2 U_0}{\partial \bar{X} \partial X} \right) \right] X \\ &+ \left( \frac{\partial F_{\text{QHA}}^{\text{vib}}}{\partial X} \right) - \left( \frac{\partial^2 U_0}{\partial X \partial \bar{X}} \right) \left( \frac{\partial^2 U_0}{\partial \bar{X} \partial \bar{X}} \right)^{-1} \left( \frac{\partial F_{\text{QHA}}^{\text{vib}}}{\partial \bar{X}} \right) = 0 \end{aligned} \quad (33)$$

as the equation for  $X$ .

Next, we consider the constrained optimization that  $\bar{X}$  is determined to optimize  $U_0$  for given configurations of  $X$ . In the lowest order,

$$\left( \frac{\partial U_0}{\partial \bar{X}} \right) \Big|_{\bar{X}=\bar{X}(X)} \simeq \left( \frac{\partial^2 U_0}{\partial \bar{X} \partial X} \right) X + \left( \frac{\partial^2 U_0}{\partial \bar{X} \partial \bar{X}} \right) \bar{X} = 0. \quad (34)$$

Hence, we get

$$\bar{X}(X) = - \left( \frac{\partial^2 U_0}{\partial \bar{X} \partial \bar{X}} \right)^{-1} \left( \frac{\partial^2 U_0}{\partial \bar{X} \partial X} \right) X. \quad (35)$$

Substituting to

$$\begin{aligned} &\left( \frac{\partial F_{\text{QHA}}(X, \bar{X}(X), T)}{\partial X} \right) \\ &= \left( \frac{\partial F_{\text{QHA}}}{\partial X} \right) + \left( \frac{\partial \bar{X}}{\partial X} \right) \left( \frac{\partial F_{\text{QHA}}}{\partial \bar{X}} \right) \end{aligned} \quad (36)$$

we get

$$\begin{aligned} &\left( \frac{\partial F_{\text{QHA}}(X, \bar{X}(X), T)}{\partial X} \right) \\ &= \left[ \left( \frac{\partial^2 U_0}{\partial X \partial X} \right) - \left( \frac{\partial^2 U_0}{\partial X \partial \bar{X}} \right) \left( \frac{\partial^2 U_0}{\partial \bar{X} \partial \bar{X}} \right)^{-1} \left( \frac{\partial^2 U_0}{\partial \bar{X} \partial X} \right) \right] X \\ &+ \left( \frac{\partial F_{\text{QHA}}^{\text{vib}}}{\partial X} \right) - \left( \frac{\partial^2 U_0}{\partial X \partial \bar{X}} \right) \left( \frac{\partial^2 U_0}{\partial \bar{X} \partial \bar{X}} \right)^{-1} \left( \frac{\partial F_{\text{QHA}}^{\text{vib}}}{\partial \bar{X}} \right). \end{aligned} \quad (37)$$

Thus, the constrained optimization, which finds the solution of Eq. (37) equal to zero, is equivalent to the full optimization of Eq. (33) at the lowest order.

### E. Calculation of pyroelectricity

We consider the effect of the static structural change for the  $T$  dependence of the electric polarization  $\mathbf{P}(T)$ :

$$P_\mu(T) = P_\mu(T=0) + \sum_{\alpha\nu} Z_{\alpha\mu\nu}^* u_{\alpha\nu}^{(0)} + \sum_{\mu_1\nu_1} d_{\mu,\mu_1\nu_1} u_{\mu_1\nu_1}, \quad (38)$$

where  $Z_{\alpha\mu\nu}^*$  is the Born effective charge, and  $d_{\mu,\mu_1\nu_1}$  is the ion-clamped piezoelectric tensor. We neglect the electron-phonon renormalization term, which originates from the thermal vibrations of the atoms [23,44,45].

The pyroelectricity is calculated by taking the temperature derivative of the spontaneous polarization:

$$\begin{aligned} p_\mu(T) &= \frac{dP_\mu(T)}{dT} \\ &= \sum_{\alpha\nu} Z_{\alpha\mu\nu}^* \frac{du_{\alpha\nu}^{(0)}}{dT} + \sum_{\mu_1\nu_1} d_{\mu,\mu_1\nu_1} \frac{du_{\mu_1\nu_1}}{dT} \\ &= p_{\text{Born},\mu}(T) + p_{\text{piezo},\mu}(T). \end{aligned} \quad (39)$$

The pyroelectricity can also be split into the primary pyroelectricity  $p^{(1)}$  and the secondary pyroelectricity  $p^{(2)}$ . The primary pyroelectricity is the clamped-lattice pyroelectricity, while the secondary pyroelectricity is the remaining part. Since  $p_{\text{piezo}}$  is zero for fixed strains,  $p_{\text{Born}}$  can be divided into the primary pyroelectricity and a part of the secondary pyroelectricity:

$$\begin{aligned} p_\mu(T) &= p_{\text{Born},\mu}(T) + p_{\text{piezo},\mu}(T) \\ &= p_\mu^{(1)}(T) + p_{\text{Born},\mu}^{(2)}(T) + p_{\text{piezo},\mu}(T). \end{aligned} \quad (41)$$

### III. SIMULATION DETAILS

The developed method is applied to the thermal expansion and pyroelectricity of wurtzite GaN and ZnO. In this section, we present the details of the calculation of these materials.

Note that we use the same setting for both materials unless stated otherwise.

### A. Calculation of the interatomic force constants

The lattice constants of the reference structures are determined by the structural optimization based on DFT;  $a = 3.2183 \text{ \AA}$  and  $c = 5.2331 \text{ \AA}$  for GaN, and  $a = 3.2359 \text{ \AA}$  and  $c = 5.2247 \text{ \AA}$  for ZnO. The  $4 \times 4 \times 2$  supercell, which contains 128 atoms, is employed for calculating the harmonic IFCs of both GaN and ZnO. The Taylor expansion of the potential energy surface is truncated at the fourth order. For calculating the anharmonic IFCs, the  $3 \times 3 \times 2$  supercell containing 72 atoms is employed. We generate 300 random configurations by uncorrelated random sampling from harmonic IFCs [46] at 500 K. The atomic forces are calculated by DFT calculations. The details of the density functional theory (DFT) calculations are explained later in this section. The IFCs are extracted from the obtained displacement-force data using adaptive LASSO implemented in the ALAMODE package [37]. The cutoff radii are set as 12 bohrs for cubic IFCs and 8 bohrs for quartic IFCs. The quartic IFCs are restricted up to three-body terms. We impose on the IFCs the acoustic sum rule (ASR), the permutation symmetry, and the space group symmetry considering the mirror images of the atoms in the supercell [35]. The fitting error of the displacement-force data was 0.7696% for GaN and 2.1930% for ZnO, which indicates that the obtained set of IFCs well captures the potential landscape.

The second- and third-order elastic constants are calculated by fitting the strain-energy relation. The crystal symmetry is used to decrease the number of strain modes to calculate [47–49]. For each strain mode, the ground state energy was calculated for 13 strained structures from  $\eta = -0.03$  to 0.03 (see Ref. [48] for the definition of  $\eta$ ). The strain-energy relation was fitted by a cubic polynomial, whose coefficients are linear transformed to elastic constants.

The strain-IFC coupling constants  $\frac{\partial \Phi_{\mu_1 \mu_2}(\mathbf{R}_1 \alpha_1, \mathbf{R}_2 \alpha_2)}{\partial u_{\mu\nu}}$  and  $\frac{\partial \Phi(0\lambda)}{\partial u_{\mu\nu}}$  are determined by finite-difference method of first order. The harmonic IFCs and the atomic forces are calculated for the six strain modes  $u_{xx} = 0.005$ ,  $u_{yy} = 0.005$ ,  $u_{zz} = 0.005$ ,  $u_{yz} = u_{zy} = 0.0025$ ,  $u_{zx} = u_{xz} = 0.0025$ , and  $u_{xy} = u_{yx} = 0.0025$ . The other entries of the displacement gradient tensor  $u_{\mu\nu}$  are zero in each strain mode. Then, the coupling constants are obtained by dividing the differences from the results at the reference structure  $u_{\mu\nu} = 0$ .

In the QHA calculations, we use  $8 \times 8 \times 8$   $q$  mesh. We do not include nonanalytic correction in calculating the  $T$ -dependent crystal structures.

### B. Settings of the DFT calculations

VASP [50] is employed for the electronic structure calculations. The PBEsol exchange-correlation functional [51] and the projector augmented wave pseudopotentials [52,53] are used. The convergence criteria of the self-consistent field loop is set to  $10^{-8}$  eV, and accurate precision mode, which suppresses egg-box effects and errors, is used to calculate the forces accurately. The basis cutoff we use is 600 eV for both materials. We use a  $4 \times 4 \times 4$  Monkhorst-Pack  $k$  mesh

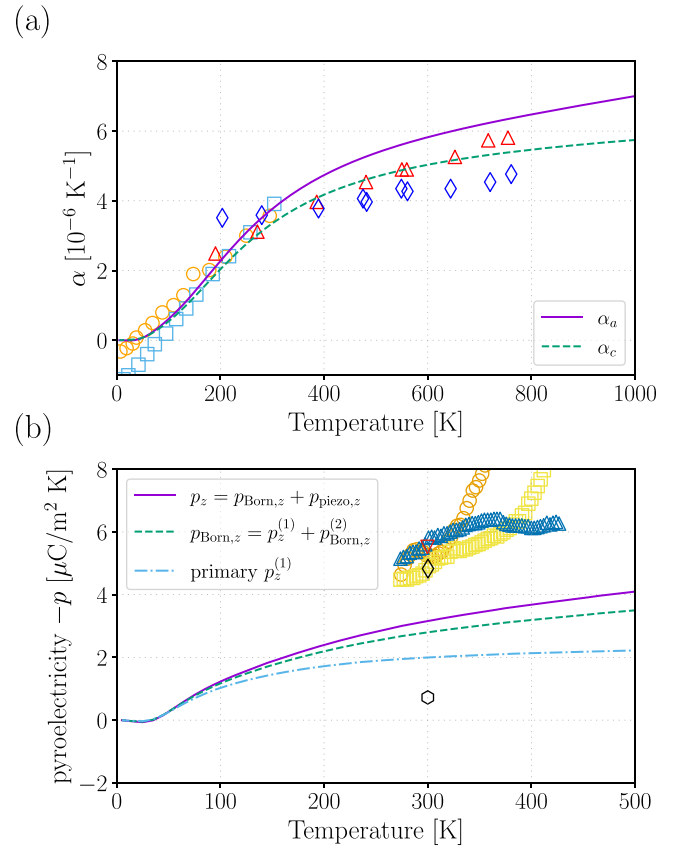


FIG. 2. The thermal expansion and the pyroelectricity of GaN calculated by QHA combined with the IFC renormalization. Both the internal coordinates and the strain are optimized to minimize the QHA free energy. (a) The thermal expansion coefficients of  $a$  and  $c$  axes ( $\alpha_a = \frac{1}{a} \frac{da}{dT}$  and  $\alpha_c = \frac{1}{c} \frac{dc}{dT}$  respectively). The experimental results are taken from Ref. [56] (orange circle for  $\alpha_a$  and cyan square for  $\alpha_c$ ) and Ref. [57] (red triangle for  $\alpha_a$  and blue diamond for  $\alpha_c$ ). (b) The purple, green, and cyan lines represent the total pyroelectricity, the Born term  $p_{\text{Born},\mu} = \sum_{\alpha\nu} Z_{\alpha\mu\nu}^* \frac{du_{\alpha\nu}^{(0)}}{dT}$ , and the primary pyroelectricity  $p_{\mu}^{(1)} = \sum_{\alpha\nu} Z_{\alpha\mu\nu}^* \left( \frac{du_{\alpha\nu}^{(0)}}{dT} \right)_{\text{fixed cell}}$ , which are defined in Sec. II E. The experimental results are taken from Ref. [58] (orange circle for the C-doped case, yellow square for the Fe-doped case, and blue triangle for the Mn-doped case), Ref. [59] (red inverted triangle), Ref. [60] (black diamond), and Ref. [61] (black hexagon).

for supercell calculations for both  $4 \times 4 \times 2$  and  $3 \times 3 \times 2$  supercells. We use the conventional DFT-based structural optimization in the primitive cell to determine the reference structure. Here, we use  $8 \times 8 \times 8$  Monkhorst-Pack  $k$  mesh, and perform structural optimization until the change of the total energy becomes less than  $10^{-7}$  eV between two consecutive steps. The Born effective charges and the clamped-lattice piezoelectricity are calculated by density functional perturbation theory [54,55] in the reference structure.

## IV. RESULTS AND DISCUSSION

### A. Finite-temperature structural optimization within QHA

We apply the developed method to the thermal expansion and the pyroelectricity of wurtzite GaN and ZnO. We first check the accuracy of the IFC renormalization, which

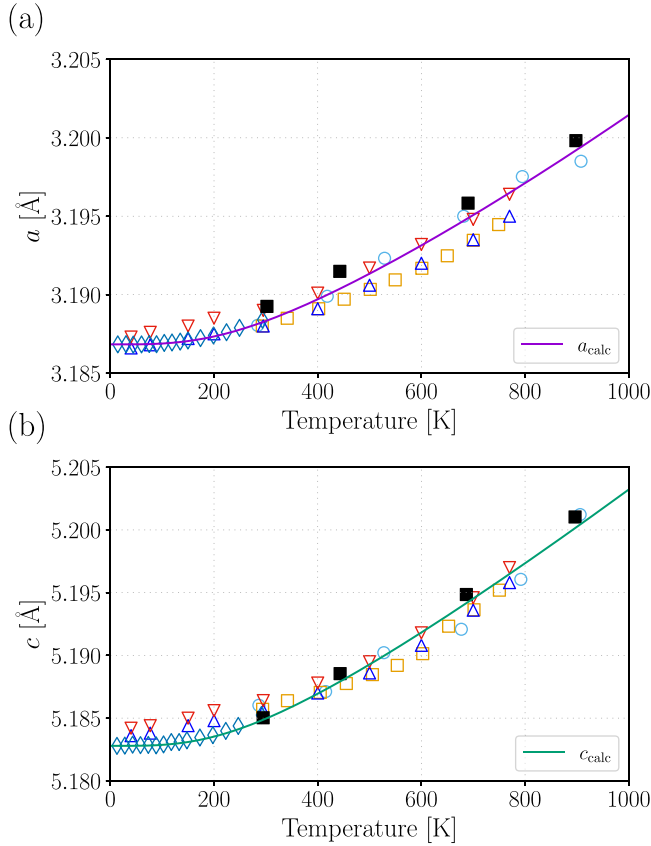


FIG. 3. The temperature dependence of the lattice constants  $a$  and  $c$  of GaN calculated by QHA combined with the IFC renormalization. Both the internal coordinates and the strain are optimized to minimize the QHA free energy. The calculation results are shifted by a constant to reproduce the experimental result at zero temperature. The experimental data are taken from Ref. [62] (cyan circle), Ref. [63] (orange square for bulk), Ref. [64] (blue triangle for bulk rough side and red inverted triangle for bulk smooth side), Ref. [65] (blue diamond), and Ref. [66] (black filled square).

is shown to reproduce the results of DFT calculations correctly. Thus, the method can be regarded as a DFT-based first-principles calculation. The result of the validations of the IFC renormalization is summarized in Sec. III in the Supplemental Material [41].

Simultaneously optimizing both the internal coordinates and the strain within QHA, we get the calculation results shown in Figs. 2–5. As seen in the figures, the thermal expansions of both GaN and ZnO are quantitatively well reproduced with our method. The thermal expansion is anisotropic, and the expansion coefficient of the lattice constant  $a$  is larger than that of  $c$ . This anisotropy is determined by a delicate interplay of internal and external degrees of freedom, which is accurately reproduced by the simultaneous optimization of all these degrees of freedom.

The calculation and experiment also show good agreement for the pyroelectricity as depicted in Figs. 2(b) and 4(b). The magnitude of the pyroelectricity is slightly underestimated for GaN. This can be because the experimental data are measured with thin films, not with bulk samples. Another possible reason is that the electron-phonon renormalization, which we

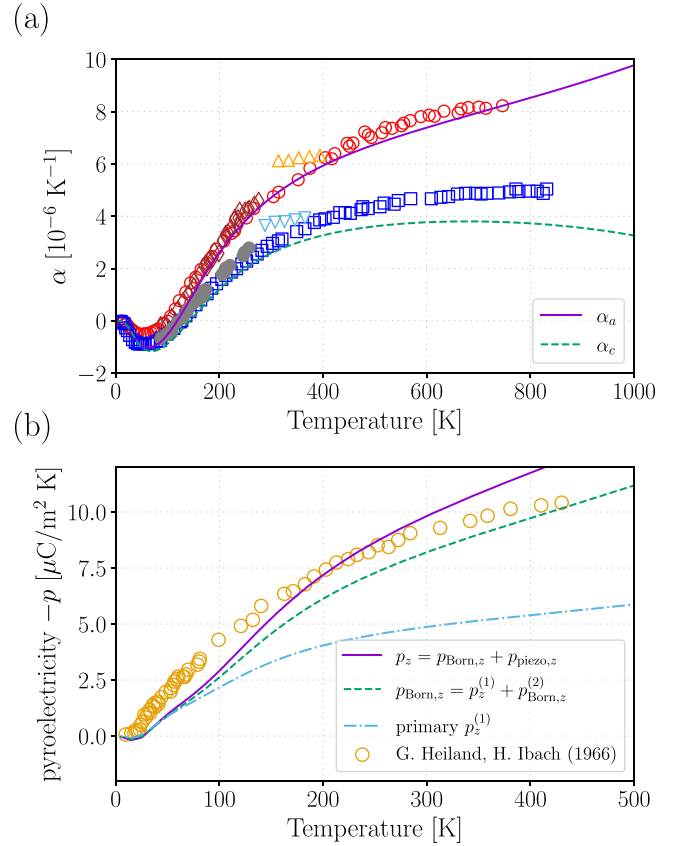


FIG. 4. The thermal expansion and the pyroelectricity of ZnO calculated by QHA combined with the IFC renormalization. Both the internal coordinates and the strain are optimized to minimize the QHA free energy. (a) The thermal expansion coefficients of  $a$  and  $c$  axes ( $\alpha_a = \frac{1}{a} \frac{da}{dT}$  and  $\alpha_c = \frac{1}{c} \frac{dc}{dT}$  respectively). The experimental data are taken from Ref. [67] (red circle for  $\alpha_a$  and blue square for  $\alpha_c$ ), Ref. [68] (orange triangle for  $\alpha_a$  and cyan inverted triangle for  $\alpha_c$ ), and Ref. [69] (brown diamond for  $\alpha_a$  and gray filled circle for  $\alpha_c$ ). (b) The purple, green, and cyan lines represent the total pyroelectricity, the Born term  $p_{\text{Born},\mu} = \sum_{\alpha\nu} Z_{\alpha\nu}^* \frac{du_{\alpha\nu}^{(0)}}{dT}$ , and the primary pyroelectricity  $p_{\mu}^{(1)} = \sum_{\alpha\nu} Z_{\alpha\nu}^* \left( \frac{du_{\alpha\nu}^{(0)}}{dT} \right)_{\text{fixed cell}}$ , which are defined in Sec. II E. The experimental data are taken from Ref. [70].

neglect in this paper, has a significant contribution, as proposed in Ref. [23].

## B. ZSISA and v-ZSISA

We perform the structural optimization using the IFC renormalization in ZSISA and v-ZSISA. The calculation results are shown in Figs. 6–9. According to Figs. 6(a) and 8(a), the thermal expansion coefficient calculated by ZSISA agrees well with the simultaneous optimization of all the degrees of freedom (full optimization). This is because ZSISA is correct at the lowest order for the  $T$  dependence of the strain [22]. From Figs. 6(b) and 8(b), we can see that  $T$ -dependent pyroelectricity calculated by ZSISA well agrees with the secondary pyroelectricity in the full optimization, which is consistent with a previous calculation [40]. As the internal coordinates are optimized at zero temperature in ZSISA, only



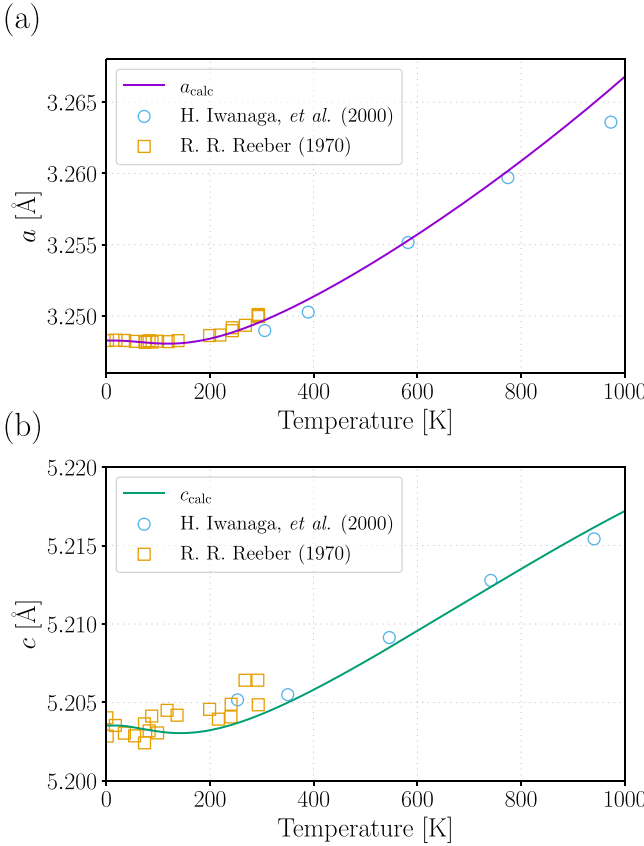


FIG. 5. The temperature dependence of the lattice constants  $a$  and  $c$  of ZnO calculated by QHA combined with the IFC renormalization. Both the internal coordinates and the strain are optimized to minimize the QHA free energy. The calculation results are shifted by a constant to reproduce the experimental result at zero temperature. The experimental data are taken from Ref. [71] (cyan circle) and Ref. [72] (orange square).

the strain-induced secondary effects are taken into account. Some works add finite temperature effect of internal coordinates afterward as a correction [23,40], which reproduces the full optimization results at the lowest order.

We next look into the results of v-ZSISA. As illustrated in Figs. 6 and 8, v-ZSISA significantly underestimates the anisotropy of the thermal expansion. As the  $T$ -dependent strain is not properly calculated, the secondary pyroelectricity is not correctly obtained either. However, as shown in Figs. 7 and 9, v-ZSISA gives precise results for the volumetric thermal expansion coefficient. Here, we note that v-ZSISA can be regarded as a special case of the constrained optimization scheme discussed in Sec. II D. Because the volume of the unit cell is

$$\begin{aligned} v_{\text{cell}}(\mathbf{u}_{\mu\nu}) &= v_{\text{cell}}(\mathbf{u}_{\mu\nu} = 0) \times \det(\mathbf{I} + \mathbf{u}_{\mu\nu}) \\ &\simeq v_{\text{cell}}(\mathbf{u}_{\mu\nu} = 0) \times (1 + \text{Tr}\mathbf{u}_{\mu\nu}), \end{aligned} \quad (42)$$

v-ZSISA corresponds to optimizing the hydrostatic strain  $\text{Tr}\mathbf{u}_{\mu\nu}$  or the cell volume at finite temperature while the other degrees of freedom are determined to minimize the DFT

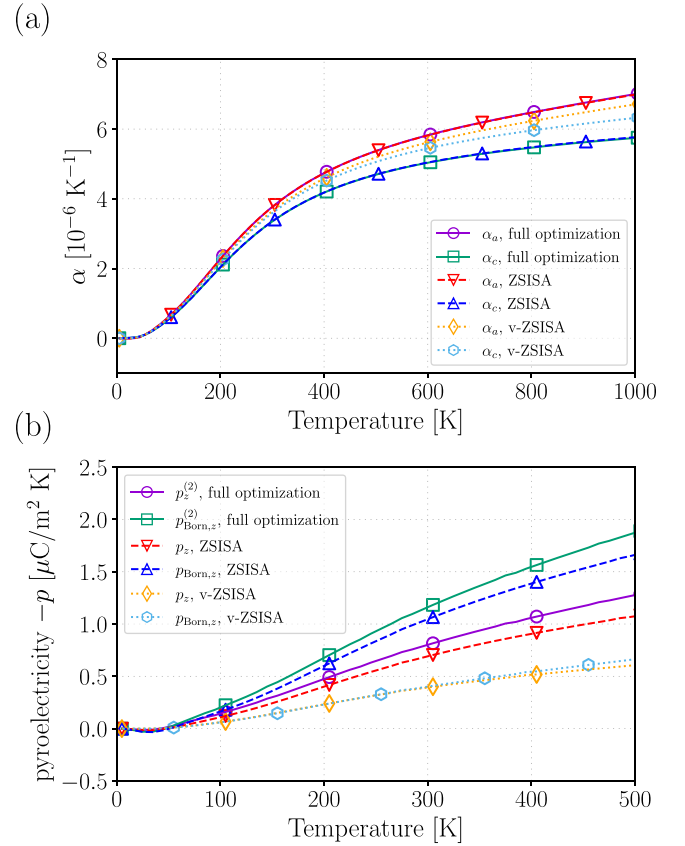


FIG. 6. The thermal expansion and the pyroelectricity of GaN calculated by QHA combined with the IFC renormalization. We compare the result of ZSISA and v-ZSISA with the result of the simultaneous optimization of the internal coordinates and the strain (full optimization). (a) The thermal expansion coefficients of  $a$  and  $c$  axes ( $\alpha_a = \frac{1}{a} \frac{da}{dT}$  and  $\alpha_c = \frac{1}{c} \frac{dc}{dT}$  respectively). The full optimization results overlap with the ZSISA results. (b) The calculation results of the pyroelectricity. The secondary pyroelectricity  $p_{\mu}^{(2)} = p_{\text{Born},\mu}^{(2)} + p_{\text{piezo},\mu} = \sum_{\alpha\nu} Z_{\alpha\mu\nu}^* \left[ \frac{du_{\alpha\nu}^{(0)}}{dT} - \left( \frac{du_{\alpha\nu}^{(0)}}{dT} \right)_{\text{fixed cell}} \right] + \sum_{\mu_1\nu_1} d_{\mu,\mu_1\nu_1} \frac{du_{\mu_1\nu_1}}{dT}$  is plotted for the full optimization case, while the total pyroelectricity  $p_z$  and the Born term  $p_{\text{Born},z}^{(2)} = \sum_{\alpha\nu} Z_{\alpha\nu z}^* \frac{du_{\alpha\nu}^{(0)}}{dT}$  are plotted for ZSISA and v-ZSISA. The different contributions to the pyroelectricity are defined in Sec. III E.

energy, which explains its success in calculating the volumetric expansion. Hence, we elucidate the range of applicability of v-ZSISA, that v-ZSISA produces reliable results for the volumetric thermal expansion but not for the anisotropy and the internal coordinates.

### C. Constrained optimization of $a$ and $c$ axes

We consider optimizing the  $a$  axis and  $c$  axis separately. Aside from the full optimization, we try three optimization schemes, which we explain for the case of calculating the  $T$  dependence of  $a$ . The first one is a special case of the constrained optimization in Sec. II D, which gives correct results for considering degrees of freedom at the lowest order. In this method, we optimize the QHA free energy with respect to  $a$  while we determine the  $a$  dependence of  $c$  and the internal coordinates by minimizing the static potential energy  $U_0$

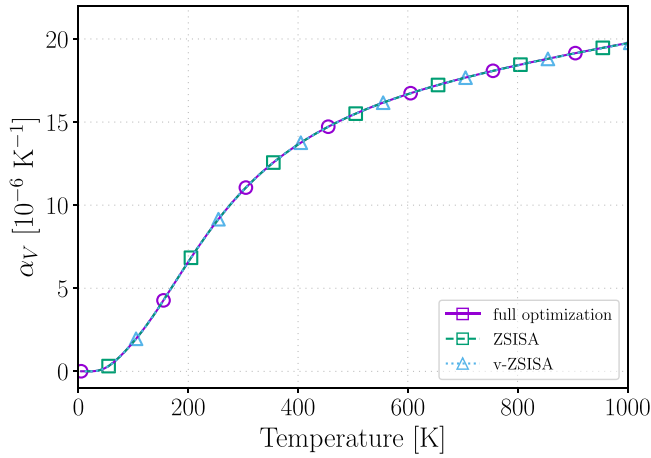


FIG. 7. The volumetric thermal expansion coefficient  $\alpha_V = \frac{1}{V} \frac{\partial V}{\partial T}$  of GaN calculated by QHA combined with IFC renormalization. We compare the result of ZSISA and v-ZSISA with the result of the simultaneous optimization of the internal coordinates and the strain (full optimization).

(constrained optimization for  $a$ ). In the other two schemes, we fix  $c$  at the value of the reference structure. The internal coordinates are also fixed in the second scheme (fixed  $u_{\alpha\mu}^{(0)}$  and  $c$ ), while they are relaxed at the ZSISA level in the third one (ZSISA, fixed  $c$ ). We try similar calculation schemes for calculating the  $T$  dependence of  $c$  as well.

The calculation results are shown in Figs. 10 and 11. As shown in Figs. 10(a) and 11(a), all the optimization schemes give similar results for  $\alpha_a$ , which is close to the result obtained by simultaneous optimization of all degrees of freedom (full optimization). Focusing on  $\alpha_c$ , the constrained optimization for  $c$  well reproduces the results of the full optimization [Fig. 10(b)], albeit not precisely for ZnO [Fig. 11(b)]. The other methods that fix  $a$  considerably overestimate the thermal expansion along the  $c$  axis. This reflects that the constrained optimization for  $c$  is correct for calculating  $T$  dependence of  $c$  in the lowest order. Note that the  $T$  dependence of degrees of freedom that are relaxed in static potential (those in  $\{\bar{X}_j\}$  in Sec. II D) significantly deviates from the full optimization results. Therefore, the constrained optimization scheme discussed in Sec. II D is useful to robustly get reasonable results by separately optimizing different degrees of freedom.

## V. CONCLUSIONS

We formulate and develop a calculation method to simultaneously optimize all structural degrees of freedom, i.e., the strain and the internal coordinates, within the QHA. Our method is based on the Taylor expansion of the potential energy surface and the IFC renormalization, which efficiently updates the IFCs with the change of crystal structures. We apply the method to the thermal expansion and the pyroelectricity of wurtzite GaN and ZnO, which shows good agreement with experiments.

Furthermore, we derive a general scheme of constrained optimization to obtain the correct  $T$  dependence of considering structural degrees of freedom at the lowest order, in which

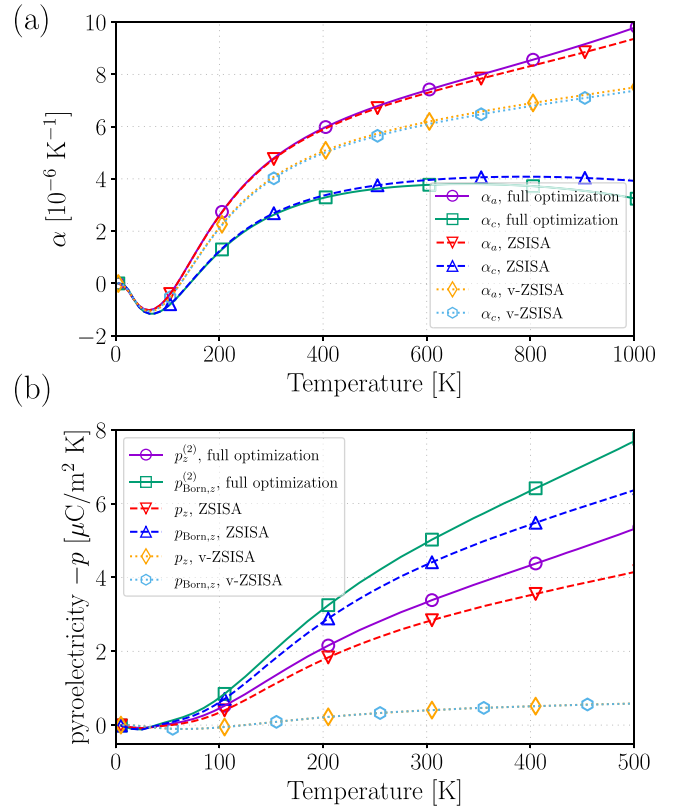


FIG. 8. The thermal expansion and the pyroelectricity of ZnO calculated by QHA combined with the IFC renormalization. We compare the result of ZSISA and v-ZSISA with the result of the simultaneous optimization of the internal coordinates and the strain (full optimization). (a) The thermal expansion coefficients of  $a$  and  $c$  axes ( $\alpha_a = \frac{1}{a} \frac{da}{dT}$  and  $\alpha_c = \frac{1}{c} \frac{dc}{dT}$  respectively). The full optimization results overlap with the ZSISA results. (b) The calculation results of the pyroelectricity. The secondary pyroelectricity  $p_\mu^{(2)} = p_{\text{Born},\mu}^{(2)} + p_{\text{piezo},\mu} = \sum_{\alpha\nu} Z_{\alpha\mu\nu}^* \left[ \frac{du_{\alpha\nu}^{(0)}}{dT} - \left( \frac{du_{\alpha\nu}^{(0)}}{dT} \right)_{\text{fixed cell}} \right] + \sum_{\mu_1\nu_1} d_{\mu,\mu_1\nu_1} \frac{du_{\mu_1\nu_1}}{dT}$  is plotted for the full optimization case, while the total pyroelectricity  $p_z$  and the Born term  $p_{\text{Born},z}^{(2)} = \sum_{\alpha\nu} Z_{\alpha\nu}^* \frac{du_{\alpha\nu}^{(0)}}{dT}$  are plotted for ZSISA and v-ZSISA. The different contributions to the pyroelectricity are defined in Sec. III E.

we optimize all the other degrees of freedom in the static potential  $U_0$ . We perform calculations using several constrained optimization schemes, such as ZSISA, v-ZSISA, and separate one-parameter optimization of  $a$  and  $c$  axes, whose results confirm the general scheme. Based on the general scheme, it is possible to reduce the optimization in the  $N_{\text{param}}$ -dimensional parameter space to  $N_{\text{param}}$  separate one-parameter optimizations, which reduces the computational cost from  $O(N_s N_{\text{param}})$  to  $O(N_s N_{\text{param}})$ , where we denote the number of sampling points of each parameter as  $N_s$ .

## ACKNOWLEDGMENTS

This work was supported by Japan Society for the Promotion of Science (JSPS) KAKENHI Grants No. 21K03424 and No. 19H05825, a Grant-in-Aid for JSPS Fellows (Grant

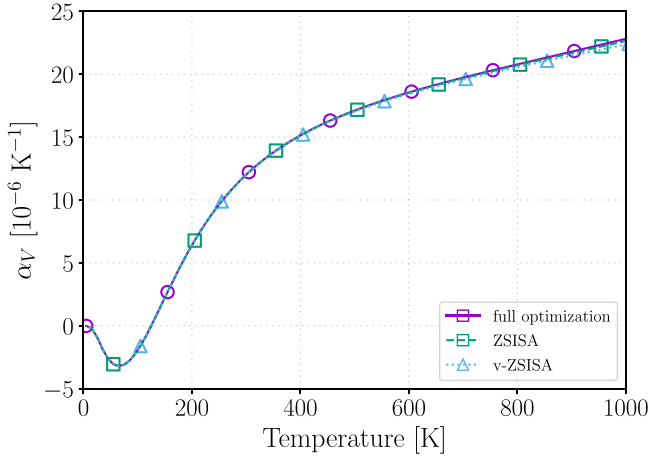


FIG. 9. The volumetric thermal expansion coefficient  $\alpha_V = \frac{1}{V} \frac{\partial V}{\partial T}$  of ZnO calculated by QHA combined with the IFC renormalization. We compare the result of ZSISA and v-ZSISA with the result of the simultaneous optimization of the internal coordinates and the strain (full optimization).

No. 22J20892), and Japan Science and Technology Agency PRESTO Grant No. JPMJPR20L7.

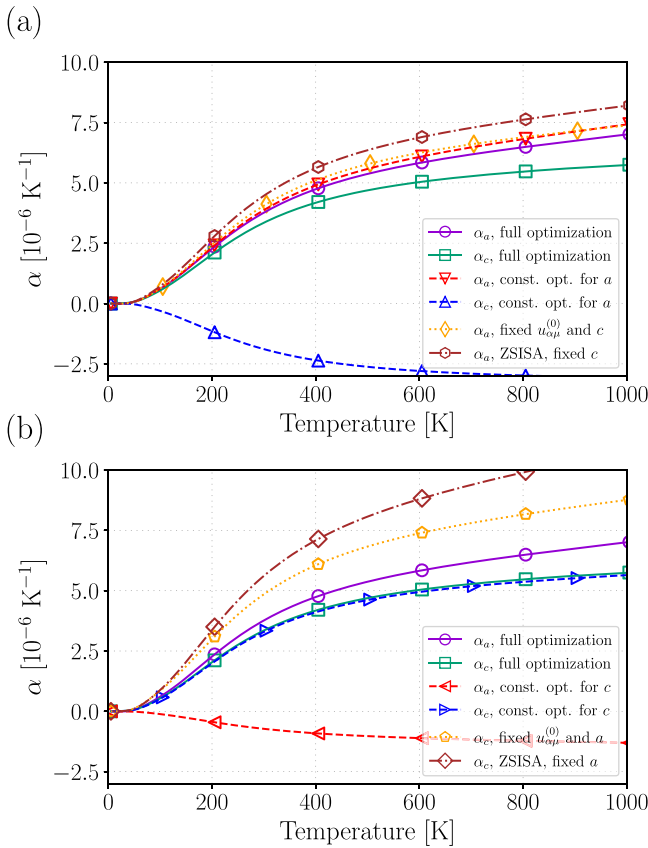


FIG. 10. The thermal expansion coefficient of GaN calculated by QHA combined with the IFC renormalization.  $\alpha_a = \frac{1}{a} \frac{da}{dT}$  and  $\alpha_c = \frac{1}{c} \frac{dc}{dT}$  are the thermal expansion coefficients of the  $a$  and  $c$  axis respectively. We compare the several schemes that separately calculate the temperature dependence of the lattice constants  $a$  and  $c$ .

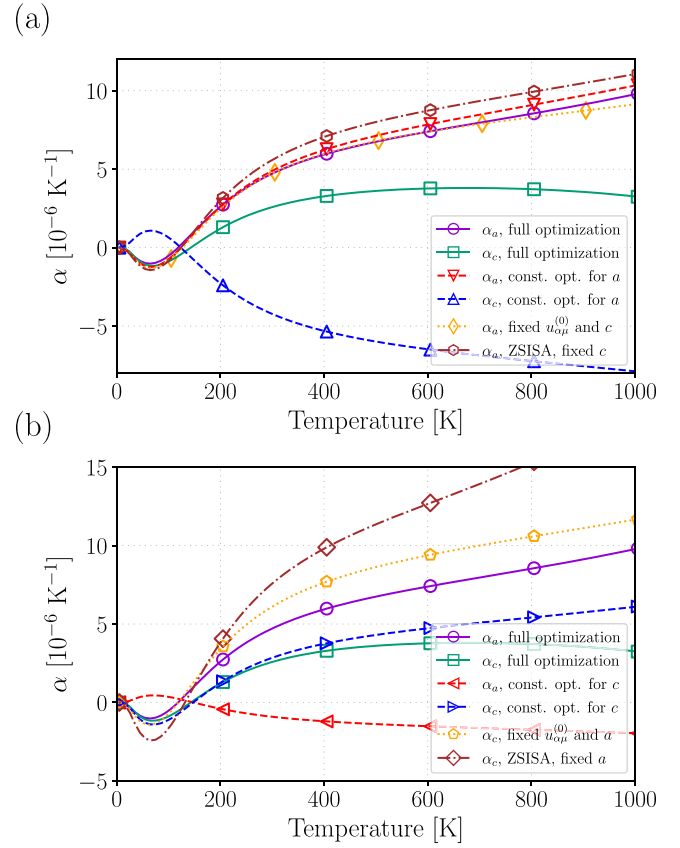


FIG. 11. The thermal expansion coefficient of ZnO calculated by QHA combined with the IFC renormalization.  $\alpha_a = \frac{1}{a} \frac{da}{dT}$  and  $\alpha_c = \frac{1}{c} \frac{dc}{dT}$  are the thermal expansion coefficients of the  $a$  and  $c$  axis respectively. We compare the several schemes that separately calculate the temperature dependence of the lattice constants  $a$  and  $c$ .

#### APPENDIX A: ROTATIONAL INVARIANCE AND ASR ON THE RENORMALIZED ATOMIC FORCES

In IFC renormalization by the strain, special care must be taken for the ASR of the first-order IFCs. In  $n$ th-order IFCs with  $n \geq 2$ , the renormalized IFCs satisfy the ASR

$$\sum_{\mathbf{R}_n \alpha_n} \Phi_{\mu_1 \dots \mu_{n-1} \mu_n}(\mathbf{0} \alpha_1, \dots, \mathbf{R}_{n-1} \alpha_{n-1}, \mathbf{R}_n \alpha_n) = 0, \quad (\text{A1})$$

if the higher-order IFCs of the reference structure satisfy the ASR. However, for the renormalized first-order IFCs to satisfy the ASR, we show that the rotational invariance on the higher-order IFCs must also be satisfied in the reference structure. Note that we assume that the IFCs in the reference structure satisfy the ASR and the permutation symmetry, which is an assumption that holds in our calculation. The space group symmetry is also imposed in the calculation, but it is not necessary for the discussion in this Appendix.

*Proposition.* For  $n \geq 2$ , assume that the IFC renormalization from the  $(n-1)$ th-order IFCs to the first-order IFCs satisfies the ASR. Then, if the rotational invariance between the  $n$ th-order and the  $(n-1)$ th-order IFCs is satisfied, the

IFC renormalization from the  $n$ th-order IFCs to the first-order IFCs satisfies the ASR.

We start from the explanation of this statement. The rotational invariance is the constraint on IFCs which comes from the invariance of the total energy for rigid rotation of the whole system. The rotational invariance is a set of constraints that connects the  $n$ th-order and the  $(n-1)$ th-order IFCs, which reads as follows: The rotational invariance between the  $n$ th-order and the  $(n-1)$ th-order IFCs is that Eq. (A2) is symmetric under the exchange of  $\mu$  and  $\nu$ :

$$\sum_{\mathbf{R}\alpha} \Phi_{\mu_1 \dots \mu_n \mu}(\mathbf{R}_1 \alpha_1, \dots, \mathbf{R}_n \alpha_n, \mathbf{R}\alpha) R_{\alpha\nu} + \sum_{i=1}^n \Phi_{\mu_i \rightarrow \mu}(\mathbf{R}_1 \alpha_1 \dots \mathbf{R}_n \alpha_n) \delta_{\mu_i \nu}, \quad (\text{A2})$$

where  $\mu_i \rightarrow \mu$  signifies  $\mu_1 \dots \mu_{i-1} \mu \mu_{i+1} \dots \mu_n$ .

$$\begin{aligned} & \sum_{\alpha_1} \sum_{\mathbf{R}_2 \alpha_2 \dots \mathbf{R}_n \alpha_n} \Phi_{\mu_1 \dots \mu_n}(\mathbf{0}\alpha_1, \mathbf{R}_2 \alpha_2, \dots, \mathbf{R}_n \alpha_n) R_{2\alpha_2 \nu_2} \dots R_{n\alpha_n \nu_n} \\ &= \sum_{\alpha_1} \sum_{\mathbf{R}_2 \alpha_2 \dots \mathbf{R}_n \alpha_n} \Phi_{\mu_1 \dots \mu_n}(\mathbf{R}_1 \alpha_1, \mathbf{R}_2 \alpha_2, \dots, \mathbf{R}_n \alpha_n) (\mathbf{R}_2 \alpha_2 - \mathbf{R}_1 \alpha_1)_{\nu_2} \dots (\mathbf{R}_n \alpha_n - \mathbf{R}_1 \alpha_1)_{\nu_n} \\ &= \sum_{\alpha_1} \sum_{\mathbf{R}_2 \alpha_2 \dots \mathbf{R}_n \alpha_n} \Phi_{\mu_1 \dots \mu_n}(\mathbf{R}_1 \alpha_1, \mathbf{R}_2 \alpha_2, \dots, \mathbf{R}_n \alpha_n) (\mathbf{R}_2 \alpha_2 - \mathbf{R}_1 \alpha_1)_{\nu_2} (\mathbf{R}_3 \alpha_3 - \mathbf{R}_2 \alpha_2)_{\nu_3} \dots (\mathbf{R}_n \alpha_n - \mathbf{R}_2 \alpha_2)_{\nu_n} \\ &= - \sum_{\alpha_1} \sum_{\mathbf{R}_2 \alpha_2 \dots \mathbf{R}_n \alpha_n} \Phi_{\mu_1 \leftrightarrow \mu_2}(\mathbf{R}_2 \alpha_2, \mathbf{R}_1 \alpha_1, \dots, \mathbf{R}_n \alpha_n) (\mathbf{R}_1 \alpha_1 - \mathbf{R}_2 \alpha_2)_{\nu_2} (\mathbf{R}_3 \alpha_3 - \mathbf{R}_2 \alpha_2)_{\nu_3} \dots (\mathbf{R}_n \alpha_n - \mathbf{R}_2 \alpha_2)_{\nu_n}. \end{aligned} \quad (\text{A5})$$

From the first line to the second line, we used the translational symmetry of the crystal lattice. From the second to the third line, we use the acoustic sum rule on the  $i$ th atom for  $i = 3, \dots, n$ . Here, we note that  $\mathbf{R}_1$  is not a dummy index but fixed somewhere in the crystal. Thus, the sum is restricted to a finite range where the atoms  $\mathbf{R}_1$  and  $\mathbf{R}_i$  interact. Although  $\mathbf{R}_{i\alpha_i} - \mathbf{R}_{j\alpha_j}$  can be infinitely large for distant atoms, the sum can be considered as a finite sum of finite elements, which is extremely important to change the order of the summation. We now fix  $\mathbf{R}_2$  instead of  $\mathbf{R}_1$ , which is allowed due to the translational symmetry. Changing the names of the dummy indices and using the translational symmetry, we get

$$\begin{aligned} & \sum_{\alpha_1} \sum_{\mathbf{R}_2 \alpha_2 \dots \mathbf{R}_n \alpha_n} \Phi_{\mu_1 \dots \mu_n}(\mathbf{0}\alpha_1, \mathbf{R}_2 \alpha_2, \dots, \mathbf{R}_n \alpha_n) R_{2\alpha_2 \nu_2} \dots R_{n\alpha_n \nu_n} \\ &= - \sum_{\alpha_1} \sum_{\mathbf{R}_2 \alpha_2 \dots \mathbf{R}_n \alpha_n} \Phi_{\mu_1 \leftrightarrow \mu_2}(\mathbf{R}_1 \alpha_1, \mathbf{R}_2 \alpha_2, \dots, \mathbf{R}_n \alpha_n) \\ & \quad \times (\mathbf{R}_2 \alpha_2 - \mathbf{R}_1 \alpha_1)_{\nu_2} \dots (\mathbf{R}_n \alpha_n - \mathbf{R}_1 \alpha_1)_{\nu_n} \\ &= - \sum_{\alpha_1} \sum_{\mathbf{R}_2 \alpha_2 \dots \mathbf{R}_n \alpha_n} \Phi_{\mu_1 \leftrightarrow \mu_2}(\mathbf{0}\alpha_1, \mathbf{R}_2 \alpha_2, \dots, \mathbf{R}_n \alpha_n) \\ & \quad \times R_{2\alpha_2 \nu_2} \dots R_{n\alpha_n \nu_n}, \end{aligned} \quad (\text{A6})$$

thus Lemma 1 has been proved.

*Lemma 2.* Assume that the IFC renormalization from the  $(n-1)$ th-order IFCs to the first-order IFCs satisfies the ASR,

The IFC renormalization from the  $n$ th-order IFCs to the first-order IFCs by the strain is

$$\frac{\partial \Phi_{\mu}(\mathbf{0}\alpha_1)}{\partial u_{\mu_2 \mu_2} \dots \partial u_{\mu_n \nu_n}} = \sum_{\{\mathbf{R}\alpha\}} \Phi_{\mu_1 \dots \mu_n}(\mathbf{0}\alpha_1, \mathbf{R}_2 \alpha_2, \dots, \mathbf{R}_n \alpha_n) \times R_{2\alpha_2 \nu_2} \dots R_{n\alpha_n \nu_n}. \quad (\text{A3})$$

Thus, the ASR on the IFC renormalization from the  $n$ th-order IFCs to the first-order IFCs is

$$\sum_{\alpha_1} \sum_{\mathbf{R}_2 \alpha_2 \dots \mathbf{R}_n \alpha_n} \Phi_{\mu_1 \dots \mu_n}(\mathbf{0}\alpha_1, \mathbf{R}_2 \alpha_2, \dots, \mathbf{R}_n \alpha_n) R_{2\alpha_2 \nu_2} \dots R_{n\alpha_n \nu_n} = 0. \quad (\text{A4})$$

Let us now move onto the proof of the proposition. We first prove the following lemma.

*Lemma 1.* The left-hand side of Eq. (A4) is antisymmetric under the exchange of  $\mu_1 \leftrightarrow \mu_2$ .

Starting from the left-hand side of Eq. (A4),

and the rotational invariance between the  $n$ th-order and the  $(n-1)$ th-order IFCs is satisfied. Then the left-hand side of Eq. (A4) is symmetric under the exchange of  $\mu_2$  and  $\nu_2$ .

Again starting from the left-hand side of Eq. (A4),

$$\begin{aligned} & \sum_{\alpha_1} \sum_{\mathbf{R}_2 \alpha_2 \dots \mathbf{R}_n \alpha_n} \Phi_{\mu_1 \dots \mu_n}(\mathbf{0}\alpha_1, \mathbf{R}_2 \alpha_2, \dots, \mathbf{R}_n \alpha_n) R_{2\alpha_2 \nu_2} \dots R_{n\alpha_n \nu_n} \\ &= \sum_{\alpha_1} \sum_{\mathbf{R}_3 \alpha_3 \dots \mathbf{R}_n \alpha_n} R_{3\alpha_3 \nu_3} \dots R_{n\alpha_n \nu_n} \\ & \quad \times \left[ \sum_{\mathbf{R}_2 \alpha_2} \Phi_{\mu_1 \dots \mu_n}(\mathbf{0}\alpha_1, \mathbf{R}_2 \alpha_2, \dots, \mathbf{R}_n \alpha_n) R_{2\alpha_2 \nu_2} \right]. \end{aligned} \quad (\text{A7})$$

Using the permutation symmetry of IFCs and the rotational invariance between the  $n$ th- and the  $(n-1)$ th-order IFCs [Eq. (A2)], we can show that Eq. (A8) below is symmetric under the exchange of  $\mu_2 \leftrightarrow \nu_2$ :

$$\begin{aligned} & \sum_{\alpha_1} \sum_{\mathbf{R}_3 \alpha_3 \dots \mathbf{R}_n \alpha_n} R_{3\alpha_3 \nu_3} \dots R_{n\alpha_n \nu_n} \\ & \quad \times \left[ \sum_{\mathbf{R}_2 \alpha_2} \Phi_{\mu_1 \dots \mu_n}(\mathbf{0}\alpha_1, \mathbf{R}_2 \alpha_2, \dots, \mathbf{R}_n \alpha_n) R_{2\alpha_2 \nu_2} \right. \\ & \quad \left. + \sum_{i \neq 2} \delta_{\mu_i \nu_2} \Phi_{\mu_i \rightarrow \mu_2}(\mathbf{0}\alpha_1, \mathbf{R}_3 \alpha_3, \dots, \mathbf{R}_n \alpha_n) \right]. \end{aligned} \quad (\text{A8})$$

The second term in the square bracket vanishes when the summation is taken due to the ASR on the IFC renormalization from the  $(n-1)$ th-order IFCs to the first-order IFCs. Lemma 2 is derived by comparing the right-hand side of Eqs. (A7) and (A8).

*Lemma 3.* Assume that the IFC renormalization from the  $(n-1)$ th-order IFCs to the first-order IFCs satisfies the ASR, and the rotational invariance between the  $n$ th-order and the  $(n-1)$ th-order IFCs is satisfied. Then the left-hand side of Eq. (A4) is symmetric under the exchange of  $\mu_1$  and  $\nu_2$ .

We show the last lemma for the proof of the proposition. We can use Lemmas 1 and 2 from the assumption of Lemma 3. Thus,

$$\begin{aligned} (\mu_1\mu_2, \nu_2) &= -(\mu_2\mu_1, \nu_2) \text{ (Lemma 1)} \\ &= -(\mu_2\nu_2, \mu_1) \text{ (Lemma 2)} \\ &= (\nu_2\mu_2, \mu_1) \text{ (Lemma 1),} \end{aligned} \quad (\text{A9})$$

where  $(\mu_1\mu_2, \nu_2)$  is a shorthand notation of the left-hand side of Eq. (A4) which focuses on the permutation of the indices  $\mu_1, \mu_2$ , and  $\nu_2$ .

*Proof of the Proposition.* Finally, we show the proof of the proposition. From Lemmas 2 and 3, we get

$$\begin{aligned} (\mu_1\mu_2, \nu_2) &= (\nu_2\mu_2, \mu_1) \text{ (Lemma 3)} \\ &= (\nu_2\mu_1, \mu_2) \text{ (Lemma 2)} \\ &= (\mu_2\mu_1, \nu_2) \text{ (Lemma 3).} \end{aligned} \quad (\text{A10})$$

On the other hand, Lemma 1 claims that

$$(\mu_1\mu_2, \nu_2) = -(\mu_2\mu_1, \nu_2) \text{ (Lemma 1).} \quad (\text{A11})$$

Therefore, from Eqs. (A10) and (A11), we get

$$(\mu_1\mu_2, \nu_2) = 0, \quad (\text{A12})$$

which proves the proposition.

In the numerical calculation, we have confirmed the IFC renormalization from the harmonic to the first-order IFCs satisfies the ASR when we impose the rotational invariance on the harmonic IFCs. On the other hand, we have checked that the IFC renormalization to the first-order IFCs from the higher-order IFCs does not satisfy the ASR if we do not impose the rotational invariance. Therefore, it is numerically demonstrated that the ASR and the permutation symmetry alone are not sufficient for the ASR on the renormalized atomic forces to be satisfied.

## APPENDIX B: IMPLEMENTATIONS OF ZSISA AND v-ZSISA

The calculation of ZSISA, which fixes the internal coordinates at the static positions in the potential energy surface, can be performed by fitting the strain dependence of the free energy after relaxing the internal coordinate in the static potential. However, in our formalism combined with the IFC renormalization, it is better to simultaneously optimize the internal and the external degrees of freedom to avoid the fitting error and to simplify the calculation scheme. In v-ZSISA, the complicated implementation of fixed-volume optimization will be a problem in calculating the volume-dependent v-ZSISA free energy to curve fit for minimization. In this

Appendix, we explain that ZSISA and v-ZSISA optimization can be performed by replacing the derivatives of QHA free energy in Eqs. (24) and (25) by appropriate functions.

We first explain the implementation of ZSISA. As the internal coordinates need to be relaxed to the static position of the potential  $U_0$ , we replace the right-hand side of Eq. (24) by

$$\frac{\partial F_{\text{QHA}}}{\partial q_\lambda^{(0)}} \rightarrow \frac{\partial F_{\text{ZSISA}}}{\partial q_\lambda^{(0)}} = \frac{\partial U_0^{(q^{(0)}, u_{\mu\nu})}}{\partial q_\lambda^{(0)}}. \quad (\text{B1})$$

It should be emphasized that ZSISA is not formulated as a global minimization of a single function of internal coordinates  $q^{(0)}$  and strain  $u_{\mu\nu}$ . Thus,  $\frac{\partial F_{\text{ZSISA}}}{\partial q_\lambda^{(0)}}$  should not be interpreted as a derivative of a function  $F_{\text{ZSISA}}$ , but is used for notational simplicity. The formula for the strain is similar to Eqs. (36) and (37) in Sec. IID. We define  $(\frac{\partial q_\lambda^{(0)}}{\partial u_{\mu\nu}})_{\text{ZSISA}}$  as the derivative in which  $q^{(0)}$  is adjusted to the strain so that the atomic forces are invariant. This definition generalizes the derivative of the true strain dependence  $q_\lambda^{(0)}(u_{\mu\nu})$  in ZSISA to arbitrary configurations of  $q_\lambda^{(0)}$  and  $u_{\mu\nu}$ . The derivative can be calculated as

$$\left(\frac{\partial q_\lambda^{(0)}}{\partial u_{\mu\nu}}\right)_{\text{ZSISA}} = -\sum_{\lambda_1} (\tilde{\Phi}_2^{-1})_{\lambda\lambda_1} \left(\frac{\partial \tilde{\Phi}(\mathbf{0}\lambda_1)}{\partial u_{\mu\nu}}\right), \quad (\text{B2})$$

where  $(\tilde{\Phi}_2^{-1})$  is the inverse matrix of  $\tilde{\Phi}(\mathbf{0}\lambda_1, \mathbf{0}\lambda_2)$  in terms of the mode indices, which can be shown in a similar way to the derivation of Eq. (35) in Sec. IID. The IFCs and the derivatives in the right-hand side of Eq. (B2) are estimated at the current structure with strain and atomic displacements. The ZSISA derivative of the free energy is

$$\frac{\partial F_{\text{ZSISA}}}{\partial u_{\mu\nu}} = \frac{\partial F_{\text{QHA}}}{\partial u_{\mu\nu}} + \sum_{\lambda} \frac{\partial F_{\text{QHA}}}{\partial q_\lambda^{(0)}} \left(\frac{\partial q_\lambda^{(0)}}{\partial u_{\mu\nu}}\right)_{\text{ZSISA}}, \quad (\text{B3})$$

with which we replace  $\frac{\partial F_{\text{QHA}}}{\partial u_{\mu\nu}}$  in Eq. (25).

In the calculation of v-ZSISA, we separate the strain to the hydrostatic strain, which causes volumetric expansion, and the deviatoric strain. The mode of the hydrostatic strain  $u_V$  is calculated as

$$\begin{aligned} u_{V,\mu\nu} &\propto \frac{\partial \det(I+u)}{\partial u_{\mu\nu}} \\ &= (I+u)_{\mu+1,\nu+1}(I+u)_{\mu+2,\nu+2} - (I+u)_{\mu+1,\nu+2} \\ &\quad \times (I+u)_{\mu+2,\nu+1}, \end{aligned} \quad (\text{B4})$$

where we use  $x=0, y=1$ , and  $z=2 \pmod{3}$  for notational simplicity. We normalize  $u_{V,\mu\nu}$  so that  $\sum_{\mu\nu} |u_{V,\mu\nu}|^2 = 1$ . Here, we calculate the structural change  $(\delta q_\lambda^{(0)v\text{-ZSISA}}, \delta u_{\mu\nu}^{v\text{-ZSISA}})$ , in which the atomic forces and the deviatoric stress tensor are unaltered in the first order. These quantities can be obtained by solving the equation

$$\begin{pmatrix} \tilde{\Phi}(\mathbf{0}\lambda, \mathbf{0}\lambda) & \frac{\partial \tilde{\Phi}(\mathbf{0}\lambda)}{\partial u_{\mu\nu}} \\ \frac{\partial \tilde{\Phi}(\mathbf{0}\lambda)}{\partial u_{\mu\nu}} & \tilde{\epsilon}_{\mu_1\nu_1, \mu_2\nu_2} \end{pmatrix} \begin{pmatrix} \delta q_\lambda^{(0)v\text{-ZSISA}} \\ \delta u_{\mu\nu}^{v\text{-ZSISA}} \end{pmatrix} \propto \begin{pmatrix} 0 \\ u_{V,\mu\nu} \end{pmatrix}, \quad (\text{B5})$$

where  $\tilde{C}_{\mu_1\nu_1, \mu_2\nu_2} = \frac{1}{N} \frac{\partial^2 U_0}{\partial u_{\mu_1\nu_1} \partial u_{\mu_2\nu_2}}$ . The matrix elements in the left-hand side of Eq. (B5) are IFC renormalized by the strain and atomic displacements. We solve the equation assuming that the tensor  $u_{\mu\nu}$  is symmetric to fix the rotational degrees of freedom. We normalize the solution of Eq. (B5) so that it satisfies

$$\sum_{\mu\nu} u_{V, \mu\nu} \delta u_{\mu\nu}^{v\text{-ZSISA}} = 1. \quad (\text{B6})$$

Then, the v-ZSISA derivative of the free energy in the direction of hydrostatic strain is

$$\begin{aligned} \frac{\partial F_{v\text{-ZSISA}}}{\partial u_V} &\propto \sum_{\mu\nu} \delta u_{\mu\nu}^{v\text{-ZSISA}} \frac{\partial F_{\text{QHA}}}{\partial u_{\mu\nu}} + \sum_{\lambda} \delta q_{\lambda}^{(0)v\text{-ZSISA}} \frac{\partial F_{\text{QHA}}}{\partial q_{\lambda}^{(0)}} \\ &= \sum_{\mu\nu} \delta u_{\mu\nu}^{v\text{-ZSISA}} \frac{\partial F_{\text{ZSISA}}}{\partial u_{\mu\nu}}. \end{aligned} \quad (\text{B7})$$

We denote the deviatoric strain modes, the modes perpendicular to  $u_V$ , as  $u_i$ . The v-ZSISA derivative of the free energy in

the direction of  $u_i$  is

$$\frac{\partial F_{v\text{-ZSISA}}}{\partial u_i} = \frac{\partial U_0^{(q^{(0)}, u_{\mu\nu})}}{\partial u_i}, \quad (\text{B8})$$

since they should be relaxed in the static potential. Transforming to the Cartesian representation, we get

$$\begin{aligned} \frac{\partial F_{v\text{-ZSISA}}}{\partial u_{\mu\nu}} &= u_{V, \mu\nu} \sum_{\mu'\nu'} \delta u_{\mu'\nu'}^{v\text{-ZSISA}} \frac{\partial F_{\text{ZSISA}}}{\partial u_{\mu'\nu'}} \\ &+ \left( \frac{\partial}{\partial u_{\mu\nu}} - u_{V, \mu\nu} \sum_{\mu'\nu'} u_{V, \mu'\nu'} \frac{\partial}{\partial u_{\mu'\nu'}} \right) U_0^{(q^{(0)}, u_{\mu\nu})}, \end{aligned} \quad (\text{B9})$$

where the normalizations of  $u_{V, \mu\nu}$  and  $\delta u_{\mu'\nu'}^{v\text{-ZSISA}}$  are assumed. The v-ZSISA derivative of the free energy in terms of the strain is

$$\frac{\partial F_{v\text{-ZSISA}}}{\partial q_{\lambda}^{(0)}} = \frac{\partial U_0^{(q^{(0)}, u_{\mu\nu})}}{\partial q_{\lambda}^{(0)}}. \quad (\text{B10})$$

The v-ZSISA optimization can be performed by replacing the right-hand side of Eqs. (24) and (25) by  $\frac{\partial F_{v\text{-ZSISA}}}{\partial q_{\lambda}^{(0)}}$  and  $\frac{\partial F_{v\text{-ZSISA}}}{\partial u_{\mu\nu}}$ , respectively.

- 
- [1] K. Takenaka, Progress of research in negative thermal expansion materials: Paradigm shift in the control of thermal expansion, *Frontiers in Chemistry* **6**, 267 (2018).
- [2] E. Liang, Q. Sun, H. Yuan, J. Wang, G. Zeng, and Q. Gao, Negative thermal expansion: Mechanisms and materials, *Front. Phys.* **16**, 53302 (2021).
- [3] W. Miller, C. W. Smith, D. S. Mackenzie, and K. E. Evans, Negative thermal expansion: A review, *J. Mater. Sci.* **44**, 5441 (2009).
- [4] C. R. Bowen, J. Taylor, E. LeBoulbar, D. Zabek, A. Chauhan, and R. Vaish, Pyroelectric materials and devices for energy harvesting applications, *Energy Environ. Sci.* **7**, 3836 (2014).
- [5] C. Wang, N. Tian, T. Ma, Y. Zhang, and H. Huang, Pyroelectric catalysis, *Nano Energy* **78**, 105371 (2020).
- [6] R. A. Surmenev, R. V. Chernozem, I. O. Pariy, and M. A. Surmeneva, A review on piezo- and pyroelectric responses of flexible nano- and micropatterned polymer surfaces for biomedical sensing and energy harvesting applications, *Nano Energy* **79**, 105442 (2021).
- [7] N. Mounet and N. Marzari, First-principles determination of the structural, vibrational and thermodynamic properties of diamond, graphite, and derivatives, *Phys. Rev. B* **71**, 205214 (2005).
- [8] B. B. Karki, R. M. Wentzcovitch, S. de Gironcoli, and S. Baroni, High-pressure lattice dynamics and thermoelasticity of MgO, *Phys. Rev. B* **61**, 8793 (2000).
- [9] E. T. Ritz and N. A. Benedek, Interplay between Phonons and Anisotropic Elasticity Drives Negative Thermal Expansion in PbTiO<sub>3</sub>, *Phys. Rev. Lett.* **121**, 255901 (2018).
- [10] M. K. Gupta, R. Mittal, and S. L. Chaplot, Negative thermal expansion in cubic ZrW<sub>2</sub>O<sub>8</sub>: Role of phonons in the entire Brillouin zone from ab initio calculations, *Phys. Rev. B* **88**, 014303 (2013).
- [11] A. Togo, L. Chaput, I. Tanaka, and G. Hug, First-principles phonon calculations of thermal expansion in Ti<sub>3</sub>SiC<sub>2</sub>, Ti<sub>3</sub>AlC<sub>2</sub>, and Ti<sub>3</sub>GeC<sub>2</sub>, *Phys. Rev. B* **81**, 174301 (2010).
- [12] P. B. Allen, Anharmonic phonon quasiparticle theory of zero-point and thermal shifts in insulators: Heat capacity, bulk modulus, and thermal expansion, *Phys. Rev. B* **92**, 064106 (2015).
- [13] P. B. Allen, Theory of thermal expansion: Quasi-harmonic approximation and corrections from quasi-particle renormalization, *Mod. Phys. Lett. B* **34**, 2050025 (2020).
- [14] R. Masuki, T. Nomoto, R. Arita, and T. Tadano, Anharmonic Grüneisen theory based on self-consistent phonon theory: Impact of phonon-phonon interactions neglected in the quasi-harmonic theory, *Phys. Rev. B* **105**, 064112 (2022).
- [15] E. Grüneisen, Theorie des festen Zustandes einatomiger Elemente, *Ann. Phys. (NY)* **344**, 257 (1912).
- [16] S. Baroni, P. Giannozzi, and E. Isaev, Density-functional perturbation theory for quasi-harmonic calculations, *Rev. Mineralogy Geochemistry* **71**, 39 (2010).
- [17] E. T. Ritz, S. J. Li, and N. A. Benedek, Thermal expansion in insulating solids from first principles, *J. Appl. Phys.* **126**, 171102 (2019).
- [18] H.-Y. Wang, H. Xu, T.-T. Huang, and C.-S. Deng, Thermodynamics of wurtzite GaN from first-principle calculation, *Eur. Phys. J. B* **62**, 39 (2008).
- [19] Y. Li, Z. D. Hood, and N. A. W. Holzwarth, Computational study of Li<sub>3</sub>BO<sub>3</sub> and Li<sub>3</sub>BN<sub>2</sub> II: Stability analysis of pure phases and of model interfaces with Li anodes, *Phys. Rev. Mater.* **5**, 085403 (2021).

- [20] A. Togo and I. Tanaka, First principles phonon calculations in materials science, *Scr. Mater.* **108**, 1 (2015).
- [21] J. M. Skelton, D. Tiana, S. C. Parker, A. Togo, I. Tanaka, and A. Walsh, Influence of the exchange-correlation functional on the quasi-harmonic lattice dynamics of II-VI semiconductors, *J. Chem. Phys.* **143**, 064710 (2015).
- [22] N. L. Allan, T. H. K. Barron, and J. A. O. Bruno, The zero static internal stress approximation in lattice dynamics, and the calculation of isotope effects on molar volumes, *J. Chem. Phys.* **105**, 8300 (1996).
- [23] J. Liu and S. T. Pantelides, Mechanisms of Pyroelectricity in Three- and Two-Dimensional Materials, *Phys. Rev. Lett.* **120**, 207602 (2018).
- [24] C. Malica and A. Dal Corso, Finite-temperature atomic relaxations: Effect on the temperature-dependent  $C_{44}$  elastic constants of Si and BAs, *J. Chem. Phys.* **156**, 194111 (2022).
- [25] J. Liu, M. V. Fernández-Serra, and P. B. Allen, First-principles study of pyroelectricity in GaN and ZnO, *Phys. Rev. B* **93**, 081205(R) (2016).
- [26] J. Liu, S. Liu, L. H. Liu, B. Hanrahan, and S. T. Pantelides, Origin of Pyroelectricity in Ferroelectric HfO<sub>2</sub>, *Phys. Rev. Appl.* **12**, 034032 (2019).
- [27] J. Liu and S. T. Pantelides, Pyroelectric response and temperature-induced  $\alpha$ - $\beta$  phase transitions in  $\alpha$ -In<sub>2</sub>Se<sub>3</sub> and other  $\alpha$ -III<sub>2</sub>VI<sub>3</sub> (III=Al, Ga, In; VI=S, Se) monolayers, *2D Mater.* **6**, 025001 (2019).
- [28] A. Erba, On combining temperature and pressure effects on structural properties of crystals with standard ab initio techniques, *J. Chem. Phys.* **141**, 124115 (2014).
- [29] P. Carrier, R. Wentzcovitch, and J. Tsuchiya, First-principles prediction of crystal structures at high temperatures using the quasiharmonic approximation, *Phys. Rev. B* **76**, 064116 (2007).
- [30] L.-F. Huang, X.-Z. Lu, E. Tennesen, and J. M. Rondinelli, An efficient ab-initio quasiharmonic approach for the thermodynamics of solids, *Comput. Mater. Sci.* **120**, 84 (2016).
- [31] P. Nath, J. J. Plata, D. Usanmaz, R. Al Rahal Al Orabi, M. Fornari, M. B. Nardelli, C. Toher, and S. Curtarolo, High-throughput prediction of finite-temperature properties using the quasi-harmonic approximation, *Comput. Mater. Sci.* **125**, 82 (2016).
- [32] N. S. Abraham and M. R. Shirts, Thermal gradient approach for the quasi-harmonic approximation and its application to improved treatment of anisotropic expansion, *J. Chem. Theory Comput.* **14**, 5904 (2018).
- [33] A. Bakare and A. Bongiorno, Enhancing efficiency and scope of first-principles quasiharmonic approximation methods through the calculation of third-order elastic constants, *Phys. Rev. Mater.* **6**, 043803 (2022).
- [34] M. A. Mathis, A. Khanolkar, L. Fu, M. S. Bryan, C. A. Dennett, K. Rickert, J. M. Mann, B. Winn, D. L. Abernathy, M. E. Manley, D. H. Hurley, and C. A. Marianetti, Generalized quasiharmonic approximation via space group irreducible derivatives, *Phys. Rev. B* **106**, 014314 (2022).
- [35] R. Masuki, T. Nomoto, R. Arita, and T. Tadano, Ab initio structural optimization at finite temperatures based on anharmonic phonon theory: Application to the structural phase transitions of BaTiO<sub>3</sub>, *Phys. Rev. B* **106**, 224104 (2022).
- [36] D. C. Wallace, Thermodynamics of crystals, *Am. J. Phys.* **40**, 1718 (1972).
- [37] T. Tadano and S. Tsuneyuki, Self-consistent phonon calculations of lattice dynamical properties in cubic SrTiO<sub>3</sub> with first-principles anharmonic force constants, *Phys. Rev. B* **92**, 054301 (2015).
- [38] F. Zhou, W. Nielson, Y. Xia, and V. Ozoliņš, Lattice Anharmonicity and Thermal Conductivity from Compressive Sensing of First-Principles Calculations, *Phys. Rev. Lett.* **113**, 185501 (2014).
- [39] F. Zhou, W. Nielson, Y. Xia, and V. Ozoliņš, Compressive sensing lattice dynamics. I. General formalism, *Phys. Rev. B* **100**, 184308 (2019).
- [40] J. Liu and P. B. Allen, Internal and external thermal expansions of wurtzite ZnO from first principles, *Comput. Mater. Sci.* **154**, 251 (2018).
- [41] See Supplemental Material at <http://link.aps.org/supplemental/10.1103/PhysRevB.107.134119> for the notation of Taylor expansion of the potential energy surface, the surface effects in renormalization of the zeroth-order IFCs, and the numerical tests on the accuracy of the IFC renormalization. The Supplemental Material also contains Refs. [73–75].
- [42] T. Tadano, Y. Gohda, and S. Tsuneyuki, Anharmonic force constants extracted from first-principles molecular dynamics: applications to heat transfer simulations, *J. Phys.: Condens. Matter* **26**, 225402 (2014).
- [43] Y. Oba, T. Tadano, R. Akashi, and S. Tsuneyuki, First-principles study of phonon anharmonicity and negative thermal expansion in ScF<sub>3</sub>, *Phys. Rev. Mater.* **3**, 033601 (2019).
- [44] M. Born, On the quantum theory of pyroelectricity, *Rev. Mod. Phys.* **17**, 245 (1945).
- [45] B. Szigeti, Temperature Dependence of Pyroelectricity, *Phys. Rev. Lett.* **35**, 1532 (1975).
- [46] D. S. Kim, O. Hellman, J. Herriman, H. L. Smith, J. Y. Y. Lin, N. Shulumba, J. L. Niedziela, C. W. Li, D. L. Abernathy, and B. Fultz, Nuclear quantum effect with pure anharmonicity and the anomalous thermal expansion of silicon, *Proc. Natl. Acad. Sci. USA* **115**, 1992 (2018).
- [47] J. Zhao, J. M. Winey, and Y. M. Gupta, First-principles calculations of second- and third-order elastic constants for single crystals of arbitrary symmetry, *Phys. Rev. B* **75**, 094105 (2007).
- [48] M. Liao, Y. Liu, S.-L. Shang, F. Zhou, N. Qu, Y. Chen, Z. Lai, Z.-K. Liu, and J. Zhu, Elastic3rd: A tool for calculating third-order elastic constants from first-principles calculations, *Comput. Phys. Commun.* **261**, 107777 (2021).
- [49] K. Brugger, Pure modes for elastic waves in crystals, *J. Appl. Phys.* **36**, 759 (1965).
- [50] G. Kresse and J. Furthmüller, Efficient iterative schemes for ab initio total-energy calculations using a plane-wave basis set, *Phys. Rev. B* **54**, 11169 (1996).
- [51] J. P. Perdew, A. Ruzsinszky, G. I. Csonka, O. A. Vydrov, G. E. Scuseria, L. A. Constantin, X. Zhou, and K. Burke, Restoring the Density-Gradient Expansion for Exchange in Solids and Surfaces, *Phys. Rev. Lett.* **100**, 136406 (2008).
- [52] P. E. Blöchl, Projector augmented-wave method, *Phys. Rev. B* **50**, 17953 (1994).
- [53] G. Kresse and D. Joubert, From ultrasoft pseudopotentials to the projector augmented-wave method, *Phys. Rev. B* **59**, 1758 (1999).
- [54] S. Baroni and R. Resta, Ab initio calculation of the macroscopic dielectric constant in silicon, *Phys. Rev. B* **33**, 7017 (1986).

- [55] M. Gajdoš, K. Hummer, G. Kresse, J. Furthmüller, and F. Bechstedt, Linear optical properties in the projector-augmented wave methodology, *Phys. Rev. B* **73**, 045112 (2006).
- [56] W. Paszkowicz, J. Domagala, J. Sokolowski, G. Kamler, S. Podsiadlo, and M. Knapp, Synchrotron radiation studies of materials, in *Proceedings of the Fifth National Symposium of Synchrotron Radiation Users*, 1999 (unpublished).
- [57] A. Sheleg and V. Savastenko, *Vestsi Akad. Navuk BSSR, Ser. Fiz, Mat. Navuk* **3**, 126 (1976).
- [58] S. Jachalke, P. Hofmann, G. Leibiger, F. S. Habel, E. Mehner, T. Leisegang, D. C. Meyer, and T. Mikolajick, The pyroelectric coefficient of free standing GaN grown by HVPE, *Appl. Phys. Lett.* **109**, 142906 (2016).
- [59] K. Matocha, T. Chow, and R. Gutmann, Positive flatband voltage shift in MOS capacitors on n-type GaN, *IEEE Electron Device Lett.* **23**, 79 (2002).
- [60] K. Matocha, V. Tilak, and G. Dunne, Comparison of metal-oxide-semiconductor capacitors on c-and m-plane gallium nitride, *Appl. Phys. Lett.* **90**, 123511 (2007).
- [61] A. D. Bykhovski, V. V. Kaminski, M. S. Shur, Q. C. Chen, and M. A. Khan, Pyroelectricity in gallium nitride thin films, *Appl. Phys. Lett.* **69**, 3254 (1996).
- [62] H. P. Maruska and J. J. Tietjen, The preparation and properties of vapor-deposited single-crystal-line GaN, *Appl. Phys. Lett.* **15**, 327 (1969).
- [63] M. Leszczyński, T. Suski, H. Teisseyre, P. Perlin, I. Grzegory, J. Jun, S. Porowski, and T. D. Moustakas, Thermal expansion of gallium nitride, *J. Appl. Phys.* **76**, 4909 (1994).
- [64] M. Leszczyński, H. Teisseyre, T. Suski, I. Grzegory, M. Boćkowski, J. Jun, B. Pałosz, S. Porowski, K. Pakuła, J. Baranowski *et al.*, Thermal expansion of GaN bulk crystals and homoepitaxial layers, *Acta Phys. Pol. A* **90**, 887 (1996).
- [65] R. R. Reeber and K. Wang, Lattice parameters and thermal expansion of GaN, *J. Mater. Res.* **15**, 40 (2000).
- [66] C. Roder, S. Einfeldt, S. Figge, and D. Hommel, Temperature dependence of the thermal expansion of GaN, *Phys. Rev. B* **72**, 085218 (2005).
- [67] H. Ibach, Thermal expansion of silicon and zinc oxide (II), *Phys. Status Solidi B* **33**, 257 (1969).
- [68] A. A. Khan, X-ray determination of thermal expansion of zinc oxide, *Acta Cryst. A* **24**, 403 (1968).
- [69] B. Yates, R. F. Cooper, and M. M. Kreitman, Low-temperature thermal expansion of zinc oxide. vibrations in zinc oxide and sphalerite zinc sulfide, *Phys. Rev. B* **4**, 1314 (1971).
- [70] G. Heiland and H. Ibach, Pyroelectricity of zinc oxide, *Solid State Commun.* **4**, 353 (1966).
- [71] H. Iwanaga, A. Kunishige, and S. Takeuchi, Anisotropic thermal expansion in wurtzite-type crystals, *J. Mater. Sci.* **35**, 2451 (2000).
- [72] R. R. Reeber, Lattice parameters of ZnO from 4.2° to 296° K, *J. Appl. Phys.* **41**, 5063 (1970).
- [73] P. Vinet, J. H. Rose, J. Ferrante, and J. R. Smith, Universal features of the equation of state of solids, *J. Phys.: Condens. Matter* **1**, 1941 (1989).
- [74] F. Birch, Finite elastic strain of cubic crystals, *Phys. Rev.* **71**, 809 (1947).
- [75] F. D. Murnaghan, The compressibility of media under extreme pressures, *Proc. Natl. Acad. Sci. USA* **30**, 244 (1944).